ATOMIC THEORY OF THE SCANNING TUNNELING MICROSCOPE

A THESIS

Submitted to the Department of Physics
and the Institute of Graduate Studies
of Bilkent University
in Partial Fulfillment of the Requirements
for the Degree of
Master of Science

By

A. Erkan TEKMAN
January, 1988

ATOMIC THEORY
OF THE
SCANNING TUNNELING
MICROSCOPE

A THESIS
SUBMITTED TO THE DEPARTMENT OF PHYSICS
AND THE INSTITUTE OF GRADUATE STUDIES
OF BİLKENT UNIVERSITY
IN PARTIAL FULFILLMENT OF THE REQUIREMENTS
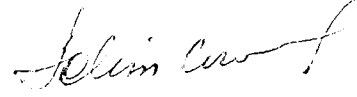FOR THE DEGREE OF
MASTER OF SCIENCE

By
A. Erkan TEKMAN   *A. Erkan Tekman*
January 1988   tarafından sağlanmıştır.

To my family...

I certify that I have read this thesis and that in my opinion it is fully adequate, in scope and quality as a dissertation for the degree of Master of Science.

Prof. Dr. Salim Çıracı
Principal Advisor

I certify that I have read this thesis and that in my opinion it is fully adequate, in scope and quality as a dissertation for the degree of Master of Science.

Prof. Dr. Cemal Yalabık

I certify that I have read this thesis and that in my opinion it is fully adequate, in scope and quality as a dissertation for the degree of Master of Science.
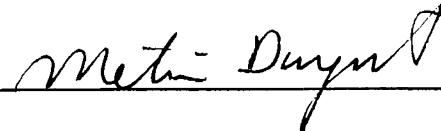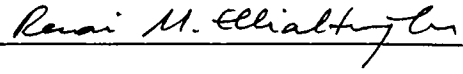
Assoc. Prof. Dr. Metin Durgut

I certify that I have read this thesis and that in my opinion it is fully adequate, in scope and quality as a dissertation for the degree of Master of Science.

_____

Assoc. Prof. Dr. Recai Ellialtıoğlu

I certify that I have read this thesis and that in my opinion it is fully adequate, in scope and quality as a dissertation for the degree of Master of Science.

_____

Assoc. Prof. Dr. Şinasi Ellialtıoğlu

Approved for the Institute of Graduate Studies

_____

Director, Institute of Graduate Studies,
Prof. Dr. Mehmet Baray

ABSTRACT

ATOMIC THEORY OF THE SCANNING TUNNELING MICROSCOPE

TEKMAN, Ahmet Erkan
M. S. in Physics
Supervisor : Prof. Dr. Salim Çıracı
January 1988, 99 pages

The Scanning Tunneling Microscope is proven to be one of the most powerful tools for surface structure determination. Present theories are able to explain the operation of the microscope when the tip is far from the surface. For the small tip height case the atomic-scale interaction of the tip and the surface has to be included in the theory. The electronic structure of the combined system of the tip and the surface is calculated with an Empirical Tight Binding approach for graphite. It is found that in the vicinity of the tip some Tip Induced Localized States are formed. These states play an important role in the tunneling phenomenon. The contribution of these states to the tunneling current is calculated.

Key words: Scanning Tunneling Microscopy, Tunneling, Empirical Tight Binding, Tip Induced Localized States, Graphite.

ÖZETÇE

TARAMA TÜNELLEME MİKROSKOBUNUN ATOMSAL KURAMI

TEKMAN, Ahmet Erkan
Yüksek Lisans Tezi, Fizik Bölümü
Tez Yöneticisi : Prof. Dr. Salim Çıracı
Ocak 1988, 99 sahife

Tarama Tünelleme Mikroskobunun yüzey yapısı belirlenmesinde güçlü bir araç olduğu ortaya çıkmıştır. Şu ana kadar öne sürülen kuramlar uç yüzeyden uzakta iken mikroskobun çalışma ilkesini açıklayabilmektedirler. Ufak uç yüksekliği durumunda uç ile yüzey arasında atomik boyuttaki etkileşimin kurama eklenmesi gerekmektedir. Uç ve yüzeyin oluşturduğu bileşik sistemin elektronik yapısı Denemesel Sıkı Bağlanma yöntemi ile grafit için hesaplandı. Uç çevresinde Uç Güdümlenmiş Yöreselleşmiş Durumlar oluştuğu bulundu. Bu durumların tünellenme olayında önemli katkılarının olduğu gözlendi. Bu durumların tünelleme akımına katkıları hesaplandı.

Anahtar sözcükler: Tarama Tünelleme Mikroskobu, Tünelleme, Denemesel sıkı Bağlanma, Uç Güdümlenmiş Yöreselleşmiş Durumlar, Grafit.

Acknowledgement

During the study on Scanning Tunneling Microscopy and preparation of this thesis my supervisor Prof. Dr. Salim Çıracı guided, helped and motivated me, with his constant decisiveness and his friendly, welcoming personality. Without his remarks, advices and ideas this study could not be completed.

I debt special thanks to Assoc. Prof. Dr. Metin Durgut, Assoc. Prof. Dr. Şinasi Ellialtıoğlu and Assoc. Prof. Dr. Recai Ellialtıoğlu for their valuable remarks and discussions on the subject.

Finally I would like to thank to the Research Assistants of the Engineering and Science Faculty of Bilkent University for their continuous morale support, especially to Oğuz Gülseren for his accompaniments while this study was on progress, and to İlhami Torunoğlu for his guiding comments on my dissertation talk.

Table of Contents

List of Figures

List of Tables

Chapter 1

Introduction

It has been known since the first years of the quantum mechanics that, particles can be found in the regions of space, which classical mechanics excludes, with a nonzero probability. This statement is a result of the wave-particle duality, and henceforth Heisenberg uncertainity principle. The tunneling phenomenon is a special demonstration of this fact. In tunneling, a particle transferred between two classically allowed regions by passing through a classically forbidden barrier region. Tunneling phenomena in solids have been investigated for a large number of different systems and is shown to be one of the basic physical events.

The first application of tunneling was done by Oppenheimer [1] in 1928 to analyze the effects of huge electric fields on hydrogen atoms. He predicted an auto-ionization as a result of the formation of a lowered potential barrier in the direction of electric field. His study on the field emission was the basis of the subsequent theories of tunneling. In 1928 Fowler and Nordheim [2] explained the field emission from metals, which was observed in 1922, but was unexplained

1

since then, using the quantum mechanical theory of tunneling. There were other applications of tunneling in nuclear and atomic physics, which were treated in late-twenties [3]. In 1930 Frenkel [4] proposed a tunneling approach to the metal-metal junction resistances, which became the basis of the later solid state tunneling experiments. Nevertheless, the solid state physics is not the only area of physics in which, tunneling plays an important role.

After mid-fifties parallel to the development of the electronic devices, tunneling experiments in solid state systems attracted interest. In 1958 the p-n tunnel diode was proposed by Esaki [5]. For this invention he was awarded the Nobel Prize in Physics in 1960. In sixties tunneling experiments were held with superconducting structures and the coupling of superconducting systems could be understood in terms of tunneling.

One of the most striking applications of tunneling was realized in early-eighties for analyzing the surface structure of solids with an atomic-scale resolution . The first Scanning Tunneling Microscope was built by G. Binnig and H. Rohrer [6,7] in 1982. Since then the microscope has been developed into a widely used precise imaging tool. After this invention Binnig and Rohrer were awarded the Nobel Prize in Physics in 1986.

The underlying physical idea for the Scanning Tunneling Microscope is just the theory of tunneling. Previous applications of tunneling in solids were

made with solid insulating barriers [3]. Therefore the electrode-barrier-electrode structure was not variable for these cases. However, if one can change the geometry of the structure the tunneling phenomenon will also differ. This change in tunneling process is related to both the change of the structure and the quantum mechanical properties of the electrodes and the barrier. When one uses a vacuum barrier, and if the quantum mechanical state of one of the electrodes is known, then one can get information about the other electrode by analyzing the change in tunneling data [8].

The Scanning Tunneling Microscope essentially consists of a metal tip, the position of which can be controlled very accurately, a vacuum barrier which can be controlled by the position of the tip, and the sample surface to be investigated. While measuring the current at different lateral positions one can attain the surface topography with atomic resolution [6,7,9].

The set-up of the Scanning Tunneling Microscope has been developed since it was first proposed [10]. Nowadays it is possible to put the mechanical part of a microscope, which has atomic resolution, into a pocket-sized apparatus. Nevertheless there are still some unexplained problems. These are mainly anomalous corrugations which are not consistent with the electronic structure or the symmetry of the surface.

Present theories of Scanning Tunneling Microscopy are derived from

3

Bardeen's formalism [11] for tunneling. In this method the electrodes are assumed to be independent of each other. However, for small tip-surface separations, the atomic scale interactions between the tip and the surface have to be included in the theory.

In this thesis I will analyze the atomic scale effects of the tip-surface interaction on tunneling. In Chapter 2 a survey of the experimental and theoretical studies on Scanning Tunneling Microscopy will be given. In Chapter 3 special emphasis will be given to one of the important cases in Scanning Tunneling Microscopy, namely graphite surface, and the effect of the tip structure. In this chapter methods of calculations, and the results for electronic structure of the tip-surface combined system will be given. The effects of these results on the tunneling will be investigated in Chapter 4. General discussions and concluding remarks will be presented in Chapter 5.

Chapter 2

A Survey of Scanning Tunneling Microscopy

2.1   Experimental Technique of Scanning Tunneling Microscopy

Originating from the idea of using a metal tip as one of the electrodes, a controllable vacuum gap as the insulating barrier, and a sample surface as the second electrode, Binnig and Rohrer [6,7,8,9] built up a basic tool for investigating the solid surfaces. The so-called Scanning Tunneling Microscope consisted of a metal tip, a piezoelectric translator for varying the position of the tip and a sample surface to be detected. The schematic setup of a Scanning Tunneling Microscope is shown in Figure 2.1.

Applying a bias to the tip with respect to the surface and carrying the tip to the close proximity of the surface with a small vacuum gap in between, there will be a tunneling current between the tip and the surface. One can change the
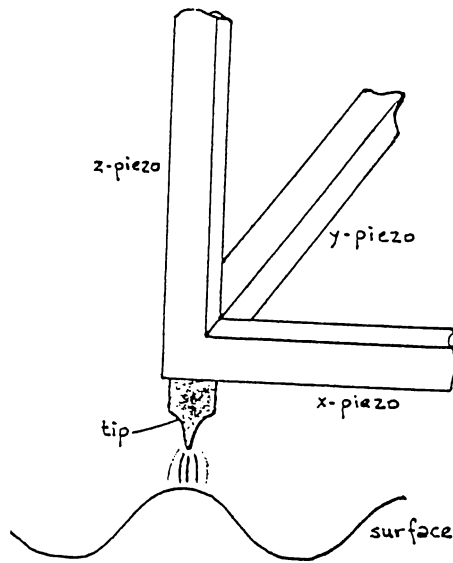
Figure 2.1: A schematic description of the scanning tunneling microscope

position of the tip with respect to the surface by using the translators, and thus

obtain the tunneling current as a function of position. It is clear that this change

in the tunneling current is closely related to the quantum mechanical state of

the surface. Therefore these scans are characteristic images of the surfaces.

Having obtained the characteristic scans, the second step for surface

structure determination is to relate them to the topographical, electronic and

other properties of the surfaces. The first interpretation of Scanning Tunneling

Microscopy was proposed by the inventors themselves [6,7]. It is clear from the

previous theoretical work on tunneling that the tunneling current from the tip to

the surface is caused by the overlapping exponential-like tails of wavefunctions

of the tip and the surface. Hence by changing the position of the tip, the

overlap of these tails will change, so will the tunneling current. Since the tip

6

wavefunction is assumed to be unaltered, the tunneling current will be related to the wavefunction of the substrate in the vicinity of the tip.

At this point one can mention the basic advantage of the Scanning Tunneling Microscope. Since the tunneling current is related to the wavefunction of the surface at the vicinity of the tip, Scanning Tunneling Microscope can make *in situ* real space measurements. There is need for neither a periodicity, as in the X-ray diffraction or Low Energy Electron Diffraction, nor a large density of states in a microscopically large area, as in the Electron Energy Loss Spectroscopy or Scanning Electron Microscopy [12]. Even small clusters like biological molecules [13] or single defects on surfaces such as adsorbates [14] or steps [7] can be observed with a good resolution.

Initially it was conjectured that when the tip is at the on-top position of one of the surface atoms, the surface wavefunction will have a large magnitude and the current will be large. Away from the on-top position the overlap of the wavefunctions and hence the current will decrease. Therefore, according to this interpretation the line scans of Scanning Tunneling Microscopy will directly reproduce the surface topography [7].

Based on the above theory the basic operation mode of the Scanning Tunneling Microscope was arranged as follows. A fixed voltage bias is applied between the tip and the surface. The height of the tip arranged to yield

a constant tunneling current while the tip scans the surface. This mode of operation is called the *constant voltage-constant current mode* [7,12] of the Scanning Tunneling Microscope. Since the tunneling current is related to the surface wavefunction, the height of the tip will be a measure of the magnitude of the wavefunction. Hence the density profile of the surface can be extracted from the scanning data.

The first Scanning Tunneling Microscope was a large apparatus [9] since some very precise supporting tools were used for isolating the system from vibrations and obtaining an ultra high vacuum. This so-called first generation Scanning Tunneling Microscope has been developed with some new considerations. Furthermore, some observations showed that the environmental disturbances may be so small that the use of simple isolating equipment would be sufficient[7,12]. Hence, nowadays for most of the applications the so-called *Pocket-Size Scanning Tunneling Microscope* [10,12] is commonly used. In addition ultra high vacuum and low temperatures are not necessary for a large variety of experiments. Therefore, experiments can be done in air [14], or even in some liquids [15,16,17] and at room temperature. These developments made the Scanning Tunneling Microscope a practical and feasible tool for surface studies. As a result, today over 200 laboratories are using Scanning Tunneling Microscopes in their studies.

In Figure 2.2 the mechanical part of a Pocket-Size Scanning Tunneling
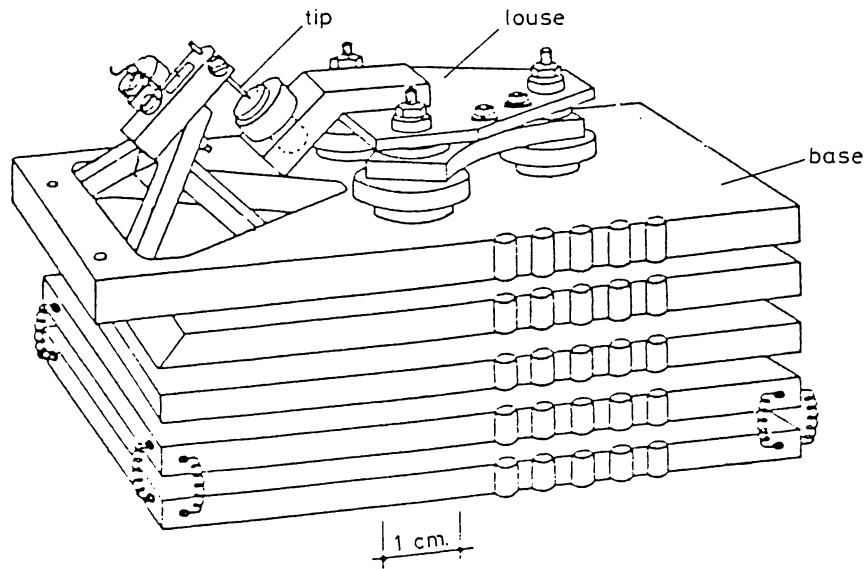
Figure 2.2: A pocket-size scanning tunneling microscope

The scale shown at the bottom corresponds to 1 cm. The drawing is taken from Reference [12]. ©1986, American Institute of Physics.

Microscope is shown. The basic parts of the microscope are as follows [12]:

1. The sample holder is attached to a stepper (louse) consisting of a tripod attached to a piezoelectric body. The louse stands on a steel plate using three anodized aluminum pods. These pods are not solidly connected to the plate, but the louse is electrostatically clamped to the plate. By setting one of the pods free and applying a voltage across the piezoelectric body to change its length one can move the feet on the plate. This procedure is applied several times to get the sample to the proximity of the tip with a coarse adjustment. The sample holder is made of a light metal such as titanium, and a few clamps are used to fix the sample on the holder.

9

2. The base of the microscope is made of a number of steel plates, separated by viton pieces for absorbing the external vibrations. This system is not effective at low temperatures and it is necessary to use more complicated vibration isolation equipments.

3. The tip holder is also made of a light metal. It is connected to a piezoelectrical tripod (scanner). Usually there are electronic units to control the x- , y- and z-scan of the tip. By applying voltages to the feet of the tripod, controllable displacements of the order of $0.1\,\mathring{A}$ can be achieved.

4. The louse, the sample holder, the scanner and the tip holder are connected to the external circuitry. Most of the operation is controlled, and the results are analyzed by a computer.

The basic operation principle of the microscope can be summarized as [12]:

1. The sample is clamped to the holder and by using the stepper, the louse is brought to the close proximity of the tip, that is to a distance of the order of 0.01 mm.

2. A constant voltage bias is applied across the tip-surface barrier. The surface is scanned while adjusting the position of the tip by using the piezo tripod keeping the tunneling current held constant, the surface is scanned. The typical scanning speed is $100\,\mathring{A}/sec$. Typical resolution of the tip position is $1\,\mathring{A}$ for x- and y-scans, and $0.1\,\mathring{A}$ for z-scan.

10

3. The resulting line scans are analyzed to obtain a grey-scale image of the surface by a computer. This is the final data of a Scanning Tunneling Microscopy experiment and includes all the information which can be collected in the constant voltage-constant current mode. The variation of tip height as a function of lateral position is called corrugation and the maximum value of corrugation is called corrugation amplitude.

2.2 Experimental Results of Scanning Tunneling Microscopy

In Section 2.1 the basic principles of the Scanning Tunneling Microscope were introduced. In this section special emphasis will be given to the experimental results which were obtained by using Scanning Tunneling Microscopy. As it was mentioned, the local character of the imaging is one of the main advantages of this microscope. Therefore it is very appropriate to use it for structure determination experiments on some complicated surfaces and molecules.

Nevertheless, the Scanning Tunneling Microscope was first used on metal surfaces [18,19]. Since the tunneling phenomenon depends on the flow of a current, it is important for the sample to have a conducting character. Because of its atomic scale resolution, the microscope is a very good candidate for determining the reconstruction of metal surfaces.

In 1983 and 1984 the inventors used Scanning Tunneling Microscopy to find the reconstruction schemes of Au (110) [18] and (100) [19] surfaces. For (110) they observed (1×2) and (1×3) reconstructed geometries, which have sawtooth like profiles consisted of energetically favorable (111) triangular facets. On the other hand, for the (100) surface several (1×5) reconstruction geometries are observed. These are the first results of Scanning Tunneling Microscopy with atomic scale resolution.

One of the most striking applications of Scanning Tunneling Microscopy is on the Si (111) surface, reconstructed in a (7×7) geometry [20]. This reconstruction scheme is hard to analyze as a result of the large unit cell, containing 49 atoms of the surface. The Scanning Tunneling Microscopy results were very accurate and consistent with the known parameters, such as the size of the 7×7 unit cell. The relief of the surface which includes two complete unit cells is shown in Figure 2.3. This pictoresque result was obtained by the inventors. In each unit cell twelve maxima and nine deep minima are observed. The minima pattern shows threefold rotational symmetry, whereas the maxima exhibit sixfold rotational symmetry around the rhombohedron corners. This result is in agreement with the "milk-stool" model of Snyder et al. [21] or the modified adatom model of Harrison [22]. As seen the imaging method has an atomic scale resolution to give a clearcut picture of the reconstruction scheme, and to guide the further research.

12
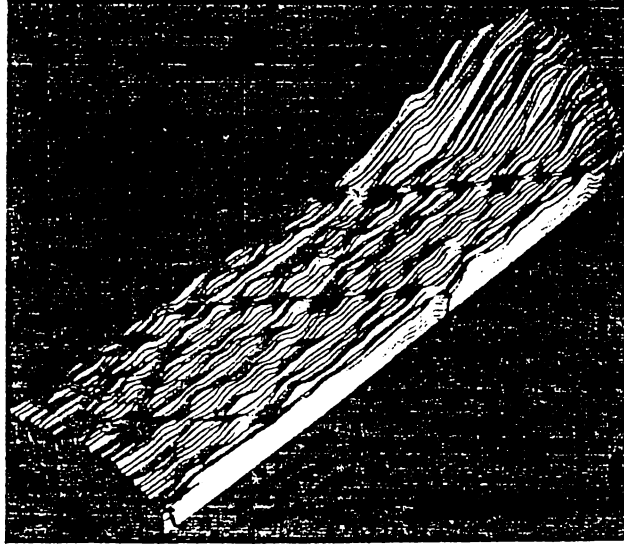
Figure 2.3: Relief of Si (111) surface-reconstructed (7 × 7)

Two complete unit cells are clearly visible with atomic scale resolution. The figure is taken from Reference [20]. ©1983, The American Physical Society.

Scanning Tunneling Microscopy is used on grating surfaces, steps and single atom defects as well [10]. The results are at least as precise as those obtained by any other surface structure determination method. Observation of single atom steps, single atom defects and adatoms with atomic scale resolution are signs for the strength of the method [7]. Even some complicated biological molecules are investigated by using a flat surface metal as a background [13]. All of these results can not be achieved by a single surface imaging tool, other than Scanning Tunneling Microscope.

The preceding examples give an idea about the power of Scanning Tunneling Microscopy for surface structure determination experiments. Nevertheless

13

there are some special cases for which the results of Scanning Tunneling Microscopy are not acceptable as far as the surface topography is concerned. The most striking example for these anomalous results is the graphite surface.

Graphite surface is one of the most easily investigated structures by using the Scanning Tunneling Microscope [10,12,14,17,23,24,25]. The surface is extremely inert as compared to the other substrates studied so far. Inertness of the surface and the distinct electronic properties lead to the atomic scale imaging under extremely varying environments. Atomic resolution is attainable in vacuum, in air [14] and when immersed in a liquid [17]. In addition to that it is very easy to prepare precisely oriented graphite surfaces, flat over microscopically large regions.

A typical Scanning Tunneling Microscopy image of the graphite surface is shown in Figure 2.4 [26]. The image was taken at a tunneling voltage of $50\,mV$. The corrugation amplitude is about $1.3\,\AA$. Owing to the symmetry properties of the graphite, which will be explained in Section 3.1.2, the honeycomb structure is not apparent in the image. Instead, two different kinds of carbon sites are found. The graphite surface is one of the structures that give most satisfactory results, excluding the small current experiments. Similar images were obtained by several groups with consistent corrugations.

In those experiments carried out with smaller bias voltages, an anomalous

14
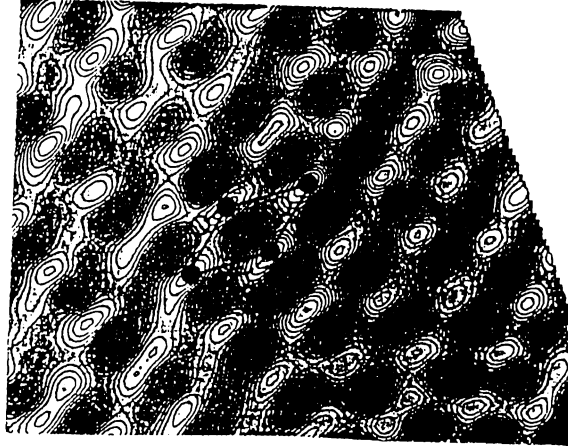
Figure 2.4: Scanning tunneling microscope image of graphite

The dark regions are corresponding to smaller current. Full lines build up the unit cell and the dashed lines show the hexagon. Full (open) circles are B-type (A-type) atoms. The asymmetry between the two basis atoms is clearly visible. The figure is taken from Reference [26]

increase in the corrugation amplitude was observed. One of these experimental results is shown in Figure 2.5 [23]. Several authors reported corrugations up to order of 10 Å [10,14,17]. It is clear that for small tunneling voltages the tip-surface separation will become smaller. Hence this giant corrugations are explainable only if this small separation regime is analyzed. In addition, there is a possibility of contamination of the tip for small tip heights. Several experimentalists reported that, it is not rare to hit the surface with the tip and take some surface atoms on the tip [14,27,28]. This situation is also common in microscopy of semiconductor surfaces. Thus, it is very difficult to have clear scans of these surfaces and to differentiate between the anomalous results.

Another structure which gives anomalous results are some the charge-
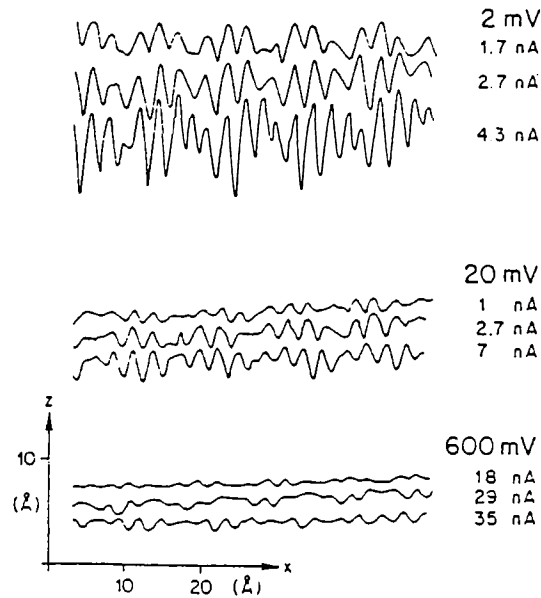
Figure 2.5: Anomalous corrugation amplitudes for graphite

The tip height is shown for one scan. The corresponding bias voltage and tunneling current are indicated. The figure is taken from Reference [23]

density wave systems [29]. For 1H-TaSe$_2$ some large corrugation amplitudes were reported. This is not the case for 2H-TaSe$_2$ structure. The explanation of these anomalous results are nearly the same as those of graphite, which will be described in detail in Section 3.1.2.

2.3 Theories for Scanning Tunneling Microscopy

As mentioned in Section 2.1 the interpretation of the Scanning Tunneling Microscopy data in terms of surface properties is one of the main objectives. The initial explanation of microscopy, assumes that the corrugation is a measure of the surface wavefunction, and thus the surface charge density. For the metallic

16

surfaces there is almost no need for further analysis since the Fermi surfaces of these materials are extended, and the local density of states is not very different from the total charge density. Hence the line scans are topographical images of the charge density, as pointed out by the inventors [6,7].

Later on Scanning Tunneling Microscopy was used on metallic surfaces with small Fermi surfaces, and even on semiconducting or insulating surfaces. For these materials the preceding explanation is no more valid, and there is a need for a general theory for Scanning Tunneling Microscopy. In order to examine tunneling from the tip to the surface in detail several models were proposed. In this Section I will give a brief summary of these theories.

One of the first ideas was directly solving the Schrödinger equation in the presence of a corrugated surface and thus calculating the tunneling current [30]. One-dimensional version of this problem is a classical subject in quantum mechanics textbooks. Garcìa et al. [30] used a highly corrugated constant potential region for modeling the tip and a smoothly corrugated constant potential region for modeling the surface. Both of the structures were taken to be periodic; the surface with a period of lateral lattice constant and the tip with a period large enough to decouple the neighboring tips. In addition, they did not use the realistic barrier potential, which includes the effects of work-function difference of the tip and the surface, image field effects and self-consistent field corrections. Instead, they used a rectangular potential barrier of height φ, which

can be thought as the average work-function of the electrodes. The solutions were expanded in terms of plane waves and the resulting matrix equation was solved. They calculated the local current distribution in the barrier and found the tunneling current expression as:

$$I = \frac{e\hbar}{2m} \; G \; N(E_F) \; V_0 \; exp \; [-2.14 \; (\frac{2m\varphi}{\hbar^2})^{1/2} \; d] \tag{2.1}$$

In this equation $N(E_F)$ is the density of states at Fermi level for the tip, V_0 is the bias applied, and d is the tip to surface distance. G is a geometrical constant, without any dependence on the other parameters.

This result is similar to those of plane surfaces, but due to the curvature of the surface there is a factor 2.14 in the exponent instead of 2 for a plane. Garcìa et al. also investigated the effects of barrier height φ and effective curvature R_{eff}, defined as the geometric average of the curvatures of the tip and the surface, on the observed corrugation amplitude. They concluded that in order to obtain the real corrugation of the surface the tip have to be very sharp. They analyzed the experimental results for Au $(110)(1 \times 2)$ reconstructed surface. They have calculated the effective tip radius as ~ 3.5 Å and the maximum tip height as ~ 3.9 Å. Their results showed that the output of Scanning Tunneling Microscopy is far from being a direct image of the surface topography, and have to be analyzed carefully to obtain the physically acceptable results.

A more extended study based on similar approximations was proposed by Stoll et al. in 1983 [31]. They used the same structure as Garcìa et al. [30] but

put emphasis on the boundary value matching, instead of solving the problem as a whole. They obtained the transmission coefficient as a function of lateral wave-vector. The sum of these contributions of all the wave-vectors yielded the total tunneling current. Using an expansion around the zero lateral wave-vector and a local approximation to the transmissivity they calculated the tunneling current as:

$$I \simeq I_i \; \frac{8 \; \pi \; \varphi \; E_{F_{eff}}}{U_{eff}^2 \; k_F} \; exp \; [-2 \; (\frac{2 \; m \; \varphi}{\hbar^2})^{1/2} \; d] \; (R_{eff}/d)^{1/2} \qquad (2.2)$$

Here $E_{F_{eff}}$ and U_{eff} are the geometrical averages of the two Fermi levels and heights of potential wells, respectively. I_i is the incident current, and R_{eff} is defined as the inverse of the arithmetic average of inverse curvatures.

Stoll et al. also obtained the local current density and tip scan curves for the constant voltage-constant current mode. They analyzed the effective radius of the tip by using the local current density. Their total current expression implies that the exponential dependence of the current on the tip height has a factor 2. Nevertheless, this approximation neglects the effects of the higher Fourier components of the incident current. Their simple fitting results in a factor of 2.08. However, they pointed out that in three dimensions this factor would be increased, and it will be close to the value found by García et al. [30] . They have found that the resolution of the microscope decreases with increasing tip size and increasing tip height.

The method described above has a computational advantage, since by

solving the Schrödinger equation using $\sim$ 20 plane waves one can get the local current distribution, and the tunneling current can be calculated easily. Nevertheless, it has some drawbacks which limit its applicability to more complicated systems. The starting point of the theory is a free-electron approximation, which assumes that the potentials are flat in the tip,surface and barrier regions and the transitions are abrupt. This approximation is reasonable for metallic electrodes. However, for semiconductors or metals with small Fermi surfaces, free-electron-like solutions are far from being realistic. In addition the use of an extended tip body with periodic large corrugations for modeling the tip may cause some artifacts. Tunneling from the tip body to the surface has to be excluded from the total tunneling current, otherwise there will be a background conductance which can lead to erroneous results. The effects of periodic tip may also cause some problems. This multi-tip model has some extra contributions to the tunneling current due to the artificial periodicity of the tip.

More recent theories originate from the quantum mechanical theory of tunneling instead of the basic quantum mechanics methods like plane-wave-like solutions. The simplest theory which can be applied to Scanning Tunneling Microscopy was proposed by Bardeen in 1961 [11]. He treated the tunneling as a transition between the many-body states of two uncoupled systems, which are interacting through a transfer Hamiltonian. Applying the first-order time-dependent perturbation theory one can find the tunneling current as:

$$I = \frac{2\,\pi\,e}{\hbar} \sum_{\mu,\nu} f(E_\mu)\,[1 - f(E_\nu + eV)]\; \mid M_{\mu\nu} \mid^2 \;\delta(E_\mu - E_\nu) \qquad (2.3)$$

where μ and ν label the tip and the surface wave-functions, respectively. Here f is the Fermi-Dirac distribution factor and takes care of the statistical probability of a particular tunneling event to happen, V is the applied bias and $M_{\mu\nu}$ is the transition matrix element between the tip state μ and the surface statue ν. Bardeen showed that this matrix element can be written as:

$$M_{\mu\nu} = \frac{\hbar^2}{2\,m} \int d\vec{S} \cdot (\psi_\mu^* \, \vec{\nabla} \, \psi_\nu - \psi_\nu \, \vec{\nabla} \, \psi_\mu^*) \qquad (2.4)$$

The integral is to be taken over any surface lying completely inside the barrier region. It is clear that the expression in the parantheses is the current operator for a general quantum mechanical system. However, one has to bear in mind the special feature of this system which is explained below.

The difference of Equation 2.3 with respect to the ordinary time-dependent perturbation theory is on the overcompleteness of the basis set. The states ψ_μ and ψ_ν are solutions of the isolated tip and surface Hamiltonians, respectively. Therefore, each set is complete and we can express the solution in terms of either one of them. However, since the tunneling is a transition between two systems separated from each other by a classically forbidden region, we can see that it is approximately equal to an element of one set at $t \to -\infty$ and to an element of the other set at $t \to \infty$. Thus, it is more appropriate to expand the tunneling solution Ψ in terms of both sets. This point will be discussed in detail in Chapter 4.

Bardeen's formalism for many-body theory of tunneling was used by

several authors for explaining Scanning Tunneling Microscopy. The most frequently referred theory for the Scanning Tunneling Microscope was proposed by Tersoff and Hamann in 1983 [32,33]. They took Bardeen's tunneling current expression as the starting point of their work. They used the following model wavefunction for the surface:

$$\psi_\nu = \Omega_s^{-1/2} \sum_G a_G \; exp[(\kappa^2 + \mid \vec{\kappa_G} \mid^2)^{1/2} \; d] \; exp(i \; \vec{\kappa_G} \cdot \vec{\rho}) \qquad (2.5)$$

where Ω_s is the normalization volume, $\kappa = \hbar^{-1}(2m\varphi)^{1/2}$, and $\vec{\kappa_G} = \vec{k_\parallel} + \vec{G}$ is the extended scheme surface state Bloch wave-vector, $\vec{\rho}$ is the lateral component of the position vector, and the summation is over the reciprocal lattice vectors of the surface. They modeled the tip as a locally spherical potential well. Taking the local curvature of the tip as the radius of the sphere and using the asymptotic spherical form of the wavefunction they found:

$$\psi_\mu = \Omega_t^{-1/2} \; c_t \; \kappa \; R \; e^{\kappa R}(\kappa \mid \vec{r} - \vec{r_0} \mid)^{-1} \; e^{(-\kappa \mid \vec{r} - \vec{r_0} \mid)} \qquad (2.6)$$

where Ω_t is the normalization volume, c_t a geometrical normalization constant of the order of one, and $\vec{r_0}$ is the position of the center of the sphere. Note that the work-functions of the tip and the surface are assumed to be the same and only the s-type wavefunction of the tip is used.

Inserting these wavefunctions into Equation 2.3 and assuming that the bias is negligibly small compared to other energy measures, they found for tunneling current to be:

$$I = 32\pi^3 \hbar^{-1} e^2 V \varphi^2 N_t(E_F) R^2 \kappa^{-4} e^{2\kappa R} \sum_\nu \mid \psi_\nu(\vec{r_0}) \mid^2 \; \delta(E_\nu - E_F) \qquad (2.7)$$

where $N_t(E_F)$ is the density of tip states at the Fermi level. In a more tractable form the tunneling conductance can be written as:

$$\sigma \; \propto \; \rho(\vec{r}_0, E_F) \qquad (2.8)$$

where $\rho(\vec{r}_0, E_F)$ is the local density of states at the Fermi level and evaluated at the position of the tip.

Tersoff and Hamann commented that the appearance of the value of surface wavefunction at the position of the center of the tip is not a physical expectation but resulted from analytic properties of the model wavefunctions used [33]. For large tip heights they also arrived to $e^{-2\kappa d}$ behavior for the tunneling current. They applied their theory to Au(110) scans for two different reconstruction schemes and had a quite good agreement with the experimental results. They also reported that Scanning Tunneling Microscopy is not sensitive to structural deviations for particular reconstructions at low voltage, that is large height regime.

Recently Chung et al. [34] included the effects of higher angular momentum states of the spherical tip in the tunneling current expression. They have found that for the case of accidental degeneracy of s- and d-states an additional current contribution from the d-state would arise and would be approximately 10% of the s-state current. They also calculated the resolution of the microscope and found that the results of completely different approaches yield similar forms.

23

This theory has a drawback about the shape of the tip. Using a sphere instead of an almost arbitrarily shaped tip with a curvature restricts the applicability of the theory. In addition, a disconnected sphere representing the tip would not have any electrical connection for a current passing through. Therefore application of Bardeen's procedure to this geometry is not totally correct, since the tip describes a quasi-stationary state instead of a sink. Recently Chen [35] used a parabolic tip for overriding this difficulty and found a tunneling current expression in terms of Kummer's functions.

Feuchtwang et al. [36] showed that the tunneling current can be found as a convolution of the tip and the surface spectral density functions. They emphasised the effects of the microscopic structure of the tip. They arrived at the conclusion that the incidence angle would be a determining factor for the effective barrier height seen by the electrons. An advantage of this method is its applicability for all types of tip structure. These results converge to those of Tersoff and Hamann in that limit. However, calculation of the spectral density functions is a tedious task and this procedure is not practical except for some special cases and requires information about the microscopic structure of the tip.

In 1984 Baratoff [37] made a review of the proposed theories and discussed some crucial points of Scanning Tunneling Microscopy. He pointed out that the electronic structure of the surface determines the completeness of the result of

24

Scanning Tunneling Spectroscopy and showed that it could be necessary to make different type of scans to get a thorough topographical image of the surface, for example to image both filled and empty bands of the semiconductor surfaces.

Baratoff also commented on the independent electrode approximation that was used by all earlier theories [37]. Actually, this is one of the most important deficiency of the theories reviewed above. This approximation can be assumed to hold for large tip heights. On the other hand, for small height cases there is a nonnegligible interaction between the tip and the surface, so that the wavefunctions used in Equation 2.3 are no more acceptable solutions.

Very recently Feuchtwang and Cutler [38] gave a survey of the studies on Scanning Tunneling Microscopy and criticized the existing theories. They also pointed out the general problems arising from the tunneling theory itself. They drew attention to the probable resonance mechanisms in Scanning Tunneling Microscopy. These mechanisms are mainly related to the image field effects such as bound states and potential resonances.

Some theories concerning the atomic aspects of the tunneling and Scanning Tunneling Microscopy were also developed. Lang [39,40,41] proposed a system for analyzing the local effects of the atoms in 1985. He used electrodes consisting of a semi-infinite jelium and an adsorbate atom. He solved the independent electrode Hamiltonians to find the states which are participating in tunneling.

25

Using these wavefunctions he found the total time dependent wavefunction Ψ_μ for the coupled two-electrode system. The current density is straightforward from basic quantum mechanics:

$$\vec{j} = V \sum_\mu \text{Im}(\Psi_\mu \, \vec{\nabla} \, \Psi_\mu^*) \, \delta(E_\mu - E_F) \qquad (2.9)$$

which reduces to:

$$\vec{j} = \pi \, V \sum_{\mu,\nu} J_{\nu\mu} \vec{j}_{\nu\mu}^* \, \delta(E_\mu - E_F) \, \delta(E_\nu - E_F) \qquad (2.10)$$

where $\vec{j}_{\nu\mu}$ and $J_{\nu\mu}$ are the local and total current operator expectation values between the tip states labeled by μ and the surface states labeled by ν, respectively. This expression is equivalent to Bardeen's formula for the tunneling current.

Lang also analyzed the effects of symmetric and energetic effects of the adsorbate atoms on the tunneling current. However, he has chosen the atom species according to their ease of computation, and therefore, his conclusions are not directly applicable to Scanning Tunneling Microscopy.

Recently Doyen and Drakova [42] used a method of chemisorption theory for describing the effect of the tip-surface interaction. They took the effects of this interaction into account by modifying the tip states. Their current expression is:

$$I = \frac{2 \, \pi \, e}{\hbar} \sum_{\mu,\mu'} S_\mu^s \, S_{\mu'}^s \, S_\mu^t \, S_{\mu'}^t \, \Delta_{\mu\mu'}^s \, \Delta_{\mu\mu'}^t \, w(\mu) \, w(\mu') \qquad (2.11)$$

26

where μ and μ' label a convenient set of orbitals localized at the vicinity of the tip and represent the outermost tip atom. S is square root of the sum of squared projections of the surface and the extended tip states on these localized orbitals. Δ's can be approximated by Kronecker deltas. $w(\mu)$ is the normalized potential element between the tip atom and the surface. They used this method for finding the scans for a step on a flat W (110) surface but as a result of the large tip height they used, they did not find any additional effect due to the tip-surface interaction.

As discussed in this section, the theory of the Scanning Tunneling Microscope is far from being complete. Every method has its own drawbacks, and as a result of the complexity of some experimental results, theories can not rigorously tested. It is clear that methods from other areas of physics will be beneficial for arriving at a conclusive theory.

A number of theoretical and experimental studies indicates the atomic nature of tunneling between the tip and the surface. Although the real tip is a very large and nonuniform cluster of atoms, the resulting corrugation images seem to be related to the outermost atom. For small tip heights one expects to have atomic scale interactions between the surface and tip atoms. The correct description lies somewhere between independent tunneling and chemisorption theory.

Chapter 3

Analysis of the Tip Induced Localized States

3.1 An Atomic Approach to Scanning Tunneling Microscopy of Graphite

3.1.1 Electronic Structure of Graphite and the Tip

As commented in Chapter 2 one has to use an atomic method to consider the interaction of the tip and the surface at small tip heights in order to analyze the reasons of anomalous results of Scanning Tunneling Microscopy. Graphite is a very appropriate candidate for this purpose, since its semi-metallic character makes it necessary to put the tip in very close proximity of the surface for obtaining reasonable tunneling currents. Therefore, graphite will be the subject matter of the rest of this work. Arguments similar to those that will be made for graphite can also be applied to other structures, such as semiconductors and other semi-metals.

Graphite has a very anisotropic crystal structure [43]. It basically consists of honeycomb-like layers, which are in turn loosely bound to the adjacent layers. The crystal structure is shown in Figure 3.1. In a layer there are two different types of carbon atom sites as far as their bonding arrangements are concerned. Half of them have carbon atoms in the neighboring layers which are directly above or below them; these are designated as A-type atoms. The other half have centers of hexagons directly above or below them; designated as B-type atoms. The nearest-neighbor distance is $a_0 = 1.418$ $\overset{\circ}{A}$ and the interlayer spacing is $c/2 = 3.348$ $\overset{\circ}{A}$. The primitive translation vectors are:

$$
\begin{aligned}
\vec{R_1} &= (\quad \sqrt{3}\,a_0 \quad, \quad 0 \quad, \ 0 \ ) \\
\vec{R_2} &= (\quad \sqrt{3}/2\,a_0 \quad, \ 3/2\,a_0 \quad, \ 0 \ ) \\
\vec{R_3} &= (\quad\quad 0 \quad\quad, \quad 0 \quad, \ c \ )
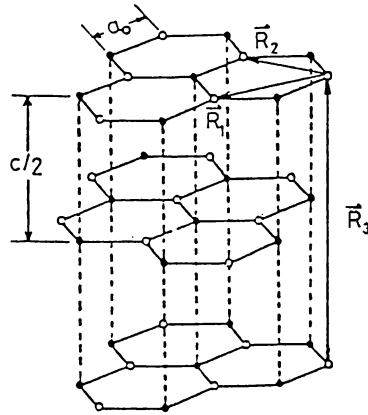\end{aligned} \tag{3.1}
$$

Figure 3.1: Structure of graphite

The dark arrows are the principal translation vectors. The full (open) circles are A-type (B-type) atoms.

The space group of graphite is $P6_3/mmc$ [43,44]. The corresponding point

29

group is isomorphic to D_{6h}. There are two inversion centers, one is halfway between the two adjacent A-type atoms, and the other is obtained from the first one by translating it in the parallel the layers by half a primitive translation vector. The local symmetry about the atoms is the same for A- and B-type atoms and is isomorphic to the group D_{3h}. The Brillouin zone of the reciprocal lattice is shown in Figure 3.2. The center of the Brillouin zone is the Γ point and the point group is D_{3h}. This group has a two-dimensional representation E' according to which (x, y) transforms. This leads to degeneracy of the p_x and p_y originated bands at the Γ point. On the line connecting Γ to H, the point group is C_{3v} and it has a two-dimensional representation, compatible with E'. At the H point on the top surface of the Brillouin zone the group is again D_{3h}. At the corner of the $k_z = 0$ cross-section of the zone, namely at K point, the point group is C_{3h}. This group has a two-dimensional representation for (x, y). Along the line connecting K to the top surface, the point group is C_3. At the top surface, P point, the point group is again C_{3v}. Along this line the two-dimensional representation is continuous.

Carbon is a tetravalent atom having a closed shell $1s$ orbital and a half-filled $2s\, 2p^3$ shell. The electronic structure of the graphite can be understood in terms of crystal structure and the electronic structure of the carbon atom. Since the interlayer spacing, c, is much greater than the nearest-neighbor distance, a_0, carbon atoms can be assumed to form bonds in the plane of the layers. Therefore, in-plane hybrid orbitals, directed on the directions of bonds will give

30
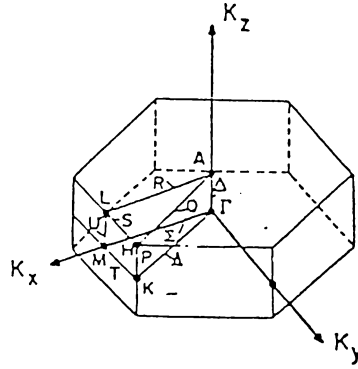
Figure 3.2: Brillouin zone of graphite

a good picture of electronic structure. These are the three $2sp^2$ hybrid orbitals, which form σ bonds. In a monolayer structure the remaining $2p_z$ orbitals[1] do not interact with the hybrids because of the different symmetries under σ_h, corresponding to the reflection in the layer plane. For the bulk graphite σ_h is not a symmetry operation , thus this separation no longer hold. For $k_z \neq 0$ there will be a non-zero interaction between these two kinds of orbitals. The p_z orbitals of the atoms on the same layer will form π bonds The small overlap of these orbitals leads to a weak van der Waals type of binding of the adjacent layers, which is essential in the formation of the crystal [43].

After this qualitative discussion on crystal binding one can look at the energy bands of graphite. The graphite monolayer has been investigated by several researchers [45]. In the monolayer the A- and B-type atoms become equivalent, the point group changes to D_{3h}. There is an inversion center located at halfway between the two nearest-neighbors. There are three special

---

[1]The z-direction is taken as perpendicular to the monolayer plane

31

symmetry points in the unit cell of graphite monolayer. The first one is the position of a monolayer atom, called the on-top position. The second one is just at the halfway between the two nearest-neighbor atoms, and is called the bridge position. The last one being the center of the hexagon is called the hollow site. This nomenclature will be used extensively in Chapters 3 and 4. For the monolayer the Brillouin zone is just the $k_z = 0$ cross-section of the bulk graphite Brillouin zone.

The graphite monolayer electronic band structure is shown in Figure 3.6. The main features of the bands are summarized as follows [43,45,46]:

- As pointed above σ and π bands, originated from sp^2 hybrids and p_z orbitals respectively, are completely decoupled. The π and π^* bands have bonding and anti-bonding character respectively. At the Brillouin zone corner K, these two bands are non-interacting and thus degenerate. This energy is the Fermi energy ($-8.0\ eV$). Hence the Fermi surface of the graphite monolayer is collapsed to a single point in the Brillouin zone, namely K. This means that graphite monolayer is a semi-metal with zero band gap.

- The remaining σ and σ^* bands are like valence and conduction bands respectively. But their energies are far from the Fermi level, thus they do not effect the electronic properties in an essential way.

- At Fermi level there are four linearly independent states. These states can be described as follows: The length of the $\vec{k}_K$ vector is one-third of a

reciprocal lattice vector. Thus, for the A-type and B-type atom sublattices the phase difference between two neighbors will be $exp(\pm i\ 2\pi/3)$. These two phase differences give two linearly independent states. Furthermore one may separate the wavefunctions of A-sublattice and B-sublattice to find four linearly independent states. If one uses, for example, a 3×3 geometry for the band calculation all four states can be identified. These states will be used in the discussion of electronic structure for the total system described in Section 3.2.2.

The bulk properties of graphite have close relations with the monolayer structure. Nonetheless there are some corrections due to the non-zero interaction between the layers, and these differences determine the actual characteristics of graphite. As mentioned above, sp^2 and p_z orbitals are interacting and as a result the bands will not be reducible for $k_z \neq 0$, however at the central plane of the Brillouin zone σ_h is a proper symmetry operation and one can separate the σ and π bands [43,44]. As a second point, interlayer interactions will cause splitting of otherwise degenerate bands. Thus Fermi surface is not simply a point, but is a cigar-like extension along K-P direction of the Brillouin zone. Also the density of states at Fermi level will be different than zero. For further information about the electronic properties of graphite, one can refer to the work of Tatar and Rabii [43].

The structure of the tip is as important as the structure of the sample. The tunneling phenomenon is governed by the electronic structures of these two

33

electrodes. In the previous theories [30,31,33,35] the tip was assumed to have some particular shapes for the sake of convenience. Since the basic aim of this study is to investigate the small separation operation of the Scanning Tunneling Microscope, it is absolutely necessary to know the microscopic structure of the tip.

The production of the tip is not controllable in the full sense. The tips are not reproducible and they deform during the microscopy or preparation. The tips are made of metals like W and Au [6,12]. In spite of that it is shown that even unreasonably different tips give meaningful results, even atomic resolution [28]. The tip is electrochemically etched from single crystal wire of diameter ~1 mm, and annealed in high electric field at a proper temperature. To have a stable tip, special emphasis have to be given to chose a low energy surface pyramid for the tip orientation. This tip is monitored by a Field Ion Microscope in the course of production. Kuk and Silverman [28] reported tips with an effective diameter of 6.3 Å. This tip had a six-atom cluster on the surface, and is appropriate for atomic resolution. Tips with monomers, dimers and trimers were unstable. After several scans the tip is often deformed by adsorption of surface atoms or by hitting to the surface. But it can be cleaned and reformed by field evaporation.

More recently Fink [47] reported a detailed study for the production of a mono-atomic tip. By using evaporation techniques he managed to form W

tips with a single atom on the surface. The Field Ion Microscopy patterns are shown in Figure 3.3. He also commented that it is possible to design tips by evaporating different kind of atoms onto the tip. But these studies are not extensively used in Scanning Tunneling Microscopy yet. Nevertheless, it is clear that the possibility of building mono-atom tips is very likely.
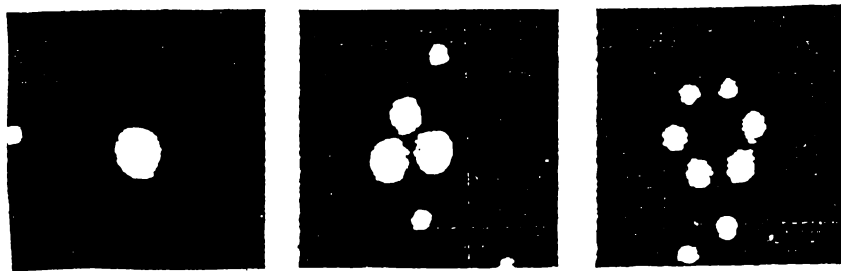
Figure 3.3: Field-ion pattern of mono-atomic tip

From left to right the first three atomic layers of the tip are shown. The layers are lifted by field evaporation. The figure is taken from Reference [47]

Even though the atomic structure of the tip can be analyzed, until now it was not possible to find its electronic structure in detail. The tip structure is very complicated, which makes a detailed account of the electronic structure difficult. This situation becomes a source of uncertainity in the tunneling mechanism. Nevertheless, the atomic structure by itself can give an idea about the possible model for the tip. In the present study a mono-atomic tip model has been used. For atomic scale resolution Park and Quate [14] remark that *"This suggests that the effective tip must consist of a single atom"*.

3.1.2 Theories for Scanning Tunneling Microscopy of Graphite

As a result of both its unusual electronic structure and appropriateness for the Scanning Tunneling Microscopy, graphite has drawn interests of both experimentalists and theoreticians. Since the first application of Scanning Tunneling Microscopy on graphite there have been a lot of suggestions about the mechanism of the anomalous tunneling current.

In 1985 Selloni et al. [48] calculated the energy band structure of graphite and found the corrugation maps for different finite biases. They used the spherical tip approximation of Tersoff and Hamann [33], and for non-zero biases used a triangular barrier for which the analytical tunneling current expression is known. They used empirical local pseudo-potential method to calculate the energy bands for a graphite slab, placed in a square potential well to approximate the surface potential. They found that by changing the bias one can tune any of the electron states to image. For infinitesimal bias, their charge density contour plots indicate that, the two basis atoms in the surface monolayer are not equivalent. However, this point was not recognized initially by Selloni et al. [48]. Corrugation amplitude for the on-top position and the hollow-site position is approximately $0.7 - 1.0$ Å. They also pointed out the possibility of observing surface states by the use of Scanning Tunneling Microscopy.

In 1986 Batra et al. [26] carried out self-consistent field calculations for

a graphite slab to investigate the Scanning Tunneling Microscopy data. Their results showed that the total charge density has a very small corrugation. In their analysis they found for the first time, that the A-type atoms have slightly smaller densities than B-type ones. They also found the local density of states at the Fermi energy. A typical local charge density plot of their results is shown in Figure 3.4. Their results for the corrugation amplitudes for this case increase up to $1.5\,\text{Å}$ between a B-type atom and the hollow-site, and are consistent with those of Selloni et al. [48]. However, they [26] observed a more pronounced difference, as large as $0.5\,\text{Å}$, between the corrugations of different types of atoms compared to $0.05\,\text{Å}$ of Selloni et al. as shown in their figures. Batra and Ciraci [49] reported similar results in a study concerning with the tip-surface interaction in Scanning Tunneling Microscopy and Atomic Force Microscopy. Batra et al. [26] also commented that the huge corrugations and loss of trigonal symmetry for the experimental results can be due to a slip of one of the planes. Some of the figures in Marti's work [12] resemble the charge densities obtained by the slipped planes. This shows that the slip plane possibility is a reasonable one.

Tersoff [50] connected the anomalous corrugation to the imaging of individual states. In 1986 he analyzed the unusual corrugations observed for the graphite and for charge-density waves in $TaSe_2$. Using the tunneling current expression he and Hamann [33] derived, he concluded that for structures with point-like Fermi surfaces, small biases image only the Fermi level state. This
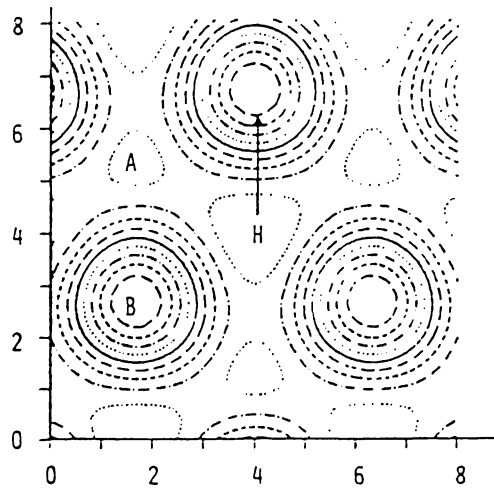
Figure 3.4: Local density of states for graphite slab

The density is calculated for a height 3.2 a.u. above the surface plane. The arrow indicates the direction on which density increases. The lateral positions are in units of a. u. . The figure is taken from Reference [26].

conclusion implies that for some structures it is almost impossible to find the topography, just by looking at the tunneling images, since Fermi level state need not have to have any basic relation with the atomic structure. Therefore it should be clear that depending on the particular system used, Scanning Tunneling Microscopy can give information about both surface geometry and electronic structure.

Tersoff [50] used a single monolayer for the graphite surface, since the interlayer interactions are very small and do not have anything to do with the anomalous corrugation. He took the six smallest reciprocal lattice vectors and expanded the local density of states in terms of these. Using Equation 2.8 he

found for the tunneling conductance:

$$\zeta = ln \ [\ \sum_{n=1}^{3} sin^2 \ \hat{\omega}_n \cdot \vec{\eta} \ ] + \zeta_0 \qquad (3.2)$$

where $\zeta = 2\kappa z_t$, z_t being the tip height, $\vec{\eta} = k_F \vec{\rho}$, $\zeta_0 = -ln(\sigma) +$ *constant* , this constant depending on the experimental and material parameters. $\hat{\omega}$ define the directions of the reciprocal lattice vectors, namely $(0,1)$, $(\frac{1}{2}\sqrt{3}, -\frac{1}{2})$, and $(-\frac{1}{2}\sqrt{3}, -\frac{1}{2})$. Using this six-plane-wave expansion he showed that there are nodes of $\rho(\vec{r}_0, E_F)$ at the hollow site of the unit cell. Which should be clear from the discussion in Section 3.1.1.

This dip at the hollow site means an infinite corrugation, and by itself is an anomalous result. However Tersoff commented that this dip is smoothened for the graphite slab due to symmetry reduction as a result of interlayer interactions [50]. In addition tip wavefunction would have some components with non-zero angular momentum around the surface normal, which will couple with the surface and give rise to a small but non-zero tunneling current.

Tersoff also found that in the six-plane-wave approximation corrugation amplitude is independent of the tip height z_t [50]. He stated that this property of graphite, while being not exact, is the reason for easy resolution of graphite surface. His results indicating that there are some examples for which Scanning Tunneling Microscopy images are not related to the topography, but are the images of individual states at Fermi level.

This anomaly for the huge corrugation amplitude in graphite is explained in terms of elastic deformations by Soler at al. [23] . They argued that the giant corrugations observed are due to the local elastic deformations, which in turn enhance the electronically based corrugation. In their experiments they observed voltage dependent corrugations and they concluded that for small tip heights the tip is practically in "physical" contact with the surface and *"It is then clear that the actual tip displacement cannot be solely a matter of the electronically induced corrugation."*. They used the standard elasticity theory to find the elastic force between the tip and the surface [23]. Their result shows that for large tip heights the force is attractive and for small heights it is repulsive. One can then qualitatively state that when the tip is on the hollow site, there will be a very small current between the tip and the surface. In order to keep the current constant the tip will move towards the surface, thus by deforming the surface like a membrane it will create a dip-like deformation on the surface. This will yield a height reading, very much below the actual tip-surface separation. When the tip is on the on-top site, there will be an attractive force between the tip and the surface and there will appear a bump on the surface. The height reading will give a value larger than the tip-surface separation. Combining these two effects one can say that there will be a giant corrugation which is not related to the electronic structure of the surface alone.

Using the local density of states formalism for the tunneling current in the geometry determined by the elastic force they obtained the corrugation
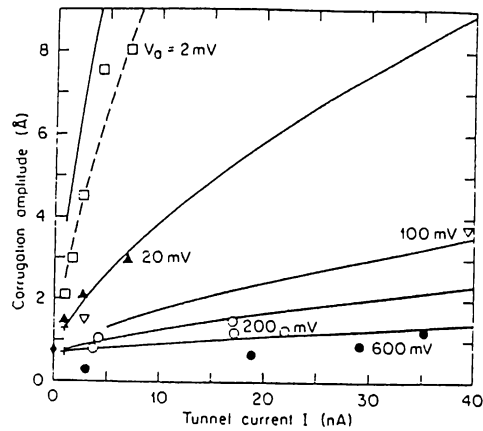
Figure 3.5: Corrugation amplitude as a function of tunneling current

The lines indicate the theoretical results. The circles, triangles and squares are experimental values. The figure is taken from Reference [23]

amplitude as a function of tunnel current. The result is shown in Figure 3.5. The agreement with experimental results is very good and on the physical basis there are reasons for the presence of this kind of mechanism. As a result of the loose interlayer binding the graphite surface is sufficiently soft for these kind of giant deformations. In addition being a semi-metal with zero energy gap, graphite can be inspected by Scanning Tunneling Microscopy only for very small tip heights, leading to a strong interaction between the tip and the surface.

Recently Ciraci and Batra [51] carried out calculations for the electronic structure of the combined tip and surface system. They found that the total energy results lead to a force regime similar to that of Soler et al. [23]. They concluded that for small tip heights the height of the barrier becomes smaller

41

and a chemical bonding between the tip and the surface becomes possible. For this case the system is short circuited to lead to the cease of tunneling.

The giant corrugation amplitude is not the only anomalous result of Scanning Tunneling Microscopy in graphite. Mizes et al. [52] recently investigated the reasons for the images with different geometries, but having the same period. Using the same argument as several other researchers [50], they neglected the effects of reciprocal wave-vectors with magnitudes greater than that of the smallest six vectors. This neglection resumes on the relation:

$$(\kappa^2 - |\vec{k}_{\parallel}|^2) = \frac{2\,m\,\varphi}{\hbar^2} \tag{3.3}$$

Therefore the decay rate of larger Fourier components is larger, and at large tip heights they will not contribute to the current. Mizes et al. [52] used a two atom tip, with a random phase difference between them. They found that the current is proportional to the sum of local densities of states at Fermi level, at the positions of the two tip atoms. Since the surface wavefunction is described by three Fourier components [50,52], the final result is the summation of two sine waves with a phase difference. They showed that by changing this phase several different patterns can be obtained as one observed in the experiment. These pattern differences have nothing to do with the structure of the surface, but is related to the structure and the orientation of the tip with respect to the surface.

Another anomalous result was obtained for gold-sputtered surfaces [24].

The gold atoms give rise to bright dots on the gray-scale output when the tip height is large. But when tip gets closer to the surface these dots diminish and the adatom becomes invisible. This case is observed by Bryant et al. [24] in 1986. They explained this anomaly with the incorporation of the gold atom into the graphite. Since gold atom wavefunctions decay into the barrier slower than graphite π bond states, their effects become apparent at large distances. However when the tip is near the surface, graphite states dominate the corrugation since the gold atom is sitting below the top layer.

Very recently Tománek et al. [25] investigated the reasons of the asymmetric corrugation for A- and B-type atoms. This asymmetry previously explained by Batra et al. [26] using the local densities of states and interlayer bonding. Tománek and coworkers commented that this inequality is not a result of local densities of states. They calculated the electronic band structure and found that π bands, localized on A-type atoms disperse along the K–P line as a result of interlayer interaction. On the other hand, bands associated with the B-type atoms are flat and at the Fermi level. This leads to imaging all B-type states in Scanning Tunneling Microscopy, and only a small fraction of A-type states due to small energy window through which tunneling occur. Their calculations gave qualitatively good result and their results are parallel to those of Batra et al. [26]. However, the tip heights they used, that is 1 $\mathring{A}$ and 0.5 $\mathring{A}$ are not appropriate to use the local density of states expression for tunneling current that will be explained in Section 3.1.2.

3.2 Energy Band Calculations and Tip In-duced Localized States

3.2.1 Method of Calculations

In this Section the tip-surface interaction at the atomic scale will be analyzed and the states which will be formed as a result of this interaction will be characterized. Since our concern is the local features of Scanning Tunneling Microscopy, a localized set of orbitals will be used. Linear Combination of Atomic Orbitals [53] method is found to be the most appropriate approach. In this method the results directly gives the atomic contributions in the eigenstates, so the characterization will be via comparison of these contributions. The actual problem is to solve the full Schrödinger equation for the system consisting of the tip and graphite. However, this system will comprises thousands of atoms, even in the vicinity of the tip. Consequently, one has to make some further approximations to get a feasible solution. The first one of these is a further simplification of the calculation method. In the Tight Binding Method [53] one has to handle some basis wavefunctions and model potentials. This will make the calculations lengthy and complicated. Therefore the Empirical Tight Binding Method [53,54] will be used, in which not the basis wavefunctions, but only the Hamiltonian matrix elements are necessary for calculation. These matrix elements can be obtained in terms of a minimal set of parameters, which

in turn fitted to results of either more realistic calculations or experiments.

In Section 3.1.1 it was noted that the graphite monolayer is a very good approximation for the bulk graphite, unless the point of interest is implicitly in the three dimensional nature of graphite. Since Scanning Tunneling Microscopy is basicly an investigation of a surface, graphite can be approximated by a single monolayer. This is a very common approximation as long as Scanning Tunneling Microscopy is considered. Note that all the experiments cited, are made on (0001) plane of the pyrolitic graphite which is the layer plane.

In Section 3.1.1 the tip structure was discussed. However, it is clear from the discussion there and in the earlier works, that the exact structure of the tip is far from being designable or even reproducible. Therefore, it is not possible to use a "real" tip model, but, a "realistic" tip model. In the earlier studies tip models are always chosen in such a way that the other approximations involved are not affected. Since the objective is to search for the atomic-scale description of Scanning Tunneling Microscopy, it is reasonable to use a few-atom tip in the calculations. This is a good approximation when the tip height is on the same order as atomic length scales. There are some comments in the literature about the tip effectively being a single atom [14,47]. A single atom tip will be used in the following calculations.

Having determined the geometry of the two parts of system,the next step

is to incorporate these two parts into a single geometry. To this end a (3×3) supercell consisting of nine graphite monolayer unit cells with a single tip atom is used. This unit of structure is repeated periodically to prevent the existence of cluster states, which are hard to analyze. There will be some effects of this artificial periodicity on the electronic states. However, the results will show that the effects of periodicity, specifically in inter-tip coupling is negligible for the (3×3) structure. In the Brillouin zone of this (3×3) unit cell the Fermi level is at the Γ point as a result of zone folding.

The next step in the present work is the determination of interaction matrix elements or energy parameters. For the sake of simplicity the non-zero interaction parameters are limited to the nearest-neighbor distance and the overlap matrix is taken to be equal to identity. This approximation leads to an eight parameters set for describing the whole monolayer bands. The σ_h symmetry operation block diagonalizes the 8×8 Hamiltonian matrix into a 2×2 and a 6×6 matrix. The p_z orbitals are interacting only between themselves, and the band dispersion for their bands is given by:

$$E_{\pi,\pi^*} = (p_z p_z)_0 \mp 3 \ (p_z p_z \pi)_1 \ [2 \ cos(\frac{2\pi\xi}{3}) \ + \ 1] \qquad (3.4)$$

where ξ is the normalized x-component of $\vec{k}$, that is $\xi = 1$ at K, the corner of the Brillouin zone. The energy parameters are:

$$\begin{aligned} (p_z p_z)_0 &= \ < p_{z1} \mid H \mid p_{z1} > \\ (p_z p_z \pi)_1 &= \ < p_{z1} \mid H \mid p_{z2} > \end{aligned} \qquad (3.5)$$

the number subscripts are for numbering the basis atoms in the unit cell. By

46

fitting the value of E_π to the results of Tatar and Rabii at the Γ and K points of the Brillouin zone, respectively, one finds:

$$
\begin{aligned}
(p_z p_z)_0 &= -8.0\,eV \\
(p_z p_z \pi)_1 &= -2.367\,eV
\end{aligned}
\tag{3.6}
$$

For the in plane orbitals the fitting problem is more complicated. The sp^2 hybrid orbitals will be used as an intermediate basis set to determine these parameters. At the Γ point of the Brillouin zone the band energies are given by the relations:

$$
\begin{aligned}
E_{\Gamma_{E'}}^{\pm} &= e_1 - e_2 \pm (e_3 + 2\,e_5) \mp (2\,e_4 + e_6) \\
E_{\Gamma_A}^{\pm} &= e_1 + 2\,e_2 \pm (e_3 + 2\,e_5) \mp 2\,(2\,e_4 + e_6
\end{aligned}
\tag{3.7}
$$

where the energy parameters e_i, are the Hamiltonian matrix elements of hybrid orbitals $\mid h_j >$. The sp^2 hybrids are defined as follows:

$$
\mathbf{h} = \mathbf{M}\,\mathbf{a}
\tag{3.8}
$$

$$
\mathbf{a} =
\begin{bmatrix}
s_1 \\
p_{x1} \\
p_{y1} \\
s_2 \\
p_{x2} \\
p_{y2}
\end{bmatrix}
\tag{3.9}
$$

$$
\mathbf{M} =
\begin{bmatrix}
\sqrt{\tfrac{1}{3}} & \sqrt{\tfrac{1}{2}} & \sqrt{\tfrac{1}{6}} & 0 & 0 & 0 \\
\sqrt{\tfrac{1}{3}} & -\sqrt{\tfrac{1}{2}} & \sqrt{\tfrac{1}{6}} & 0 & 0 & 0 \\
\sqrt{\tfrac{1}{3}} & 0 & \sqrt{\tfrac{2}{3}} & 0 & 0 & 0 \\
0 & 0 & 0 & \sqrt{\tfrac{1}{3}} & -\sqrt{\tfrac{1}{2}} & -\sqrt{\tfrac{1}{6}} \\
0 & 0 & 0 & \sqrt{\tfrac{1}{3}} & \sqrt{\tfrac{1}{2}} & -\sqrt{\tfrac{1}{6}} \\
0 & 0 & 0 & \sqrt{\tfrac{1}{3}} & 0 & \sqrt{\tfrac{2}{3}}
\end{bmatrix}.
\tag{3.10}
$$

and the matrix elements e_i are defined as:

$$
\begin{aligned}
e_1 &= <h_1 \mid \mathbf{H} \mid h_1> \\
e_2 &= <h_1 \mid \mathbf{H} \mid h_2> \\
e_3 &= <h_1 \mid \mathbf{H} \mid h_4> \\
e_4 &= <h_1 \mid \mathbf{H} \mid h_5> \\
e_6 &= <h_2 \mid \mathbf{H} \mid h_5> \\
e_6 &= <h_2 \mid \mathbf{H} \mid h_6>
\end{aligned}
\tag{3.11}
$$

From Equation 3.7 one can fix e_1 and e_2 and can find two equations in terms of remaining e_i's. At the other high symmetry points of the Brillouin zone energy eigenvalues are very hard to calculate, so it is convenient to use a least square fitting method for adjusting the values of the remaining two independent parameters. The result is then transformed back to the atomic orbital basis by using the relation:

$$
\mathbf{H}' = \mathbf{M}^T \, \mathbf{a} \, \mathbf{M}
\tag{3.12}
$$

due to the orthogonality of M. The fitted parameters are given in Table 3.1 and the band structure obtained by using this parameters is shown in Figure 3.6. The identification of the parameters is made in Reference [53]. The σ bands have a root-mean-square error of $0.20eV$ along the symmetry directions shown, and maximum error is $1.21eV$.

An important remark about the determination of interaction parameters is the invariance of the intralayer and intra-tip energy parameters as a result of the tip-surface interactions. These parameters have to change accordingly, as a result of the new diagonalization in terms of the original states, as well. However, these changes are coming from the self-consistent field effects. Since the method used is not a self-consistent one, and also the results are not

Table 3.1: Fitted Hamiltonian matrix elements (eV)

i	$(ss)_i$	$(sp)_i$	$(pp\pi)_i$	$(pp\sigma)_i$
0	-10.73	0	-6.13	0
1	-5.41	5.59	5.844	-2.018

predicting any abrupt transition, as a first order approximation, the above assumption holds.

This completes the determination of the monolayer energy parameters of graphite. Now the tip parameters and the tip-monolayer interaction parameters have to be found. At this point the use of the real extended tip will be made. As explained in Chapter 2, the experiment is carried out with a bias voltage applied across the barrier, between the metallic tip and the sample surface. Since the applied voltage will determine the energy levels of the tip with respect to the graphite, one can assume that the orbital energies of the tip atom will be shifted with respect to the graphite energy levels accordingly. Thus it is sufficient to determine the positions of these orbital energies, for example, with respect to the Fermi level of the tip.

In order to determine these energy differences it is necessary to have a knowledge about the atomic structure of the tip. However, as noted earlier, the tip structure is neither unique, nor controllable. Moreover, it is impossible to
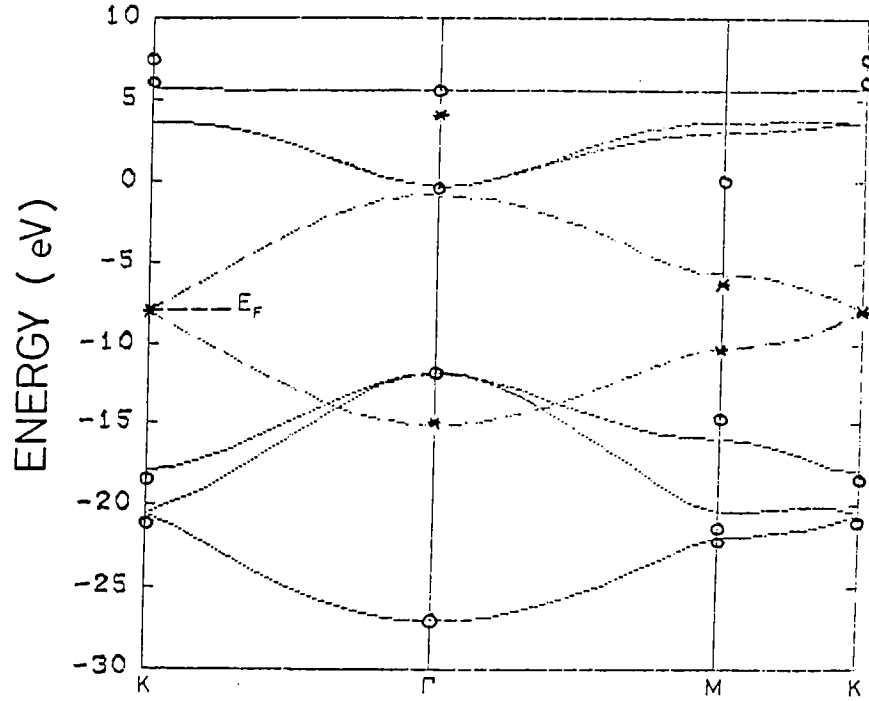
Figure 3.6: Electronic energy band structure of graphite monolayer

The bands are calculated by using the parameters listed in Table 3.1. The full lines are σ and σ^* bands, while the dashed ones are π and π^* bands. The circles and the stars pointing the energy values at symmetry points taken from Reference [43].

determine the structure *in situ*. Therefore one has to make some approximations about the tip. In Section 2.3 it was stated that for most of the theoretical work the tip and surface work-functions are taken to be equal. The experimentalists, on the other hand, report that in experiments with surfaces, for which tip height is very small, the tip is contaminated by the surface atoms [27]. Therefore it is a good approximation to take the outermost tip atoms of the same species as the surface atoms. Accordingly, a carbon atom is used as the tip, in conjuction with these observations. Since the tunneling phenomenon comprises only the states near the Fermi level it is sufficient to shift the p_z orbital energy of the

Table 3.2: The model wavefunctions and scaling

$$\phi_s(\vec{r}) = (\frac{\mu_s^3}{\pi})^{1/2} \ e^{-\mu_s \ r}$$

$$\phi_\alpha(\vec{r}) = (\frac{\mu_p^3}{\pi})^{1/2} \ \mu_p \ r_\alpha \ e^{-\mu_p \ r} \qquad \alpha = x, y, z$$

$\mu_{ss} = \mu_s$	1.6083
$\mu_{pp} = \mu_p$	1.5679
$\mu_{sp} = \frac{\mu_s + \mu_p}{2}$	1.5881

The μ values are taken from Reference [55]

tip atom to $E_F = -8.0 \ eV$. Other orbital energies are shifted accordingly, as if the differences are equal to those in a graphite monolayer.

The parameters defining the tip-monolayer interaction need a special care. As a result of uncertainty in the tip structure it is very hard to find a "real" expression for this interaction. However, one can again find "realistic" expressions. Since the tip atom is taken to be a carbon atom, its interaction with the graphite monolayer will be similar to intralayer interactions. On the other hand, in order to investigate the electronic band structure of the system with varying tip height, one has to scale the interaction parameters accordingly. This scaling can be done by using some exponentially decaying model wavefunctions for orbitals. For this purpose Slater type wavefunctions are used and the exponential factors are taken from Clementi and Raimondi's [55] study on the

screening constant. The wavefunction and the exponential factors are given in Table 3.2. When the tip-monolayer atom internuclear separation, d_{ts} is equal to the intralayer nearest-neighbor distance, a_0, it is assumed that:

$$
\begin{aligned}
(ss)_{ts} &= (ss)_1 \\
(sp)_{ts} &= (sp)_1 \\
(pp\pi)_{ts} &= (p_z p_z \pi)_1
\end{aligned}
\tag{3.13}
$$

where the subscript ts stands for tip-surface interaction. Note that for $p - p$ interactions, the monolayer p_z orbitals are taken as the starting point since they are more likely to be extended into vacuum than sp^2 like orbitals which form stronger bonds. This assumption leaves the value of $(pp\sigma)_{ts}$ undetermined. For calculating this parameter the simple argument of Harrison [53] about the comparison of free-electron and Bloch wave dispersions is used. The related expression is:

$$
(pp\sigma)_{ts} = -4 \ (pp\pi)_{ts}
\tag{3.14}
$$

The resulting parameters are also listed in Table 3.2. When tip-monolayer atom separation is different than a_0, the above parameters are scaled by the factor:

$$
exp[-\mu_{ij} \ (d_{ts} - a_0)]
\tag{3.15}
$$

The tip-surface interaction is not limited only to the nearest-neighbors. Since the tip atom p_z orbital is assumed to be a free orbital without any strong binding to the other tip atoms, this orbital is more like to interact with several atoms. From the above cited work one can find μ_{ss} and μ_{pp}, for μ_{sp} the arithmetic average of the first two is used.

Determining the energy parameters one can built up the Hamiltonian for the complete system and diagonalize it. For this purpose the standard method of band theory for Empirical Tight Binding calculations is used. The detailed description of this method is given by Slater and Koster [54].

3.2.2 Results of Calculations

Using the Empirical Tight Binding method described in Section 3.2.1 the electronic band structure for the combined monolayer-tip system is calculated for different configurations. The results lead to identification of a new class of states, namely Tip Induced Localized States. Owing to the interaction between the tip and the surface at small tip heights, the degeneracy of the states mainly localized at the tip and the surface are lifted. These states hybridized to form new bonding and anti-bonding like states in the vicinity of the tip. The energies and the orbital characters of these states strongly depend on the lateral position of the tip in addition to its height. Thus it can be concluded that the formation of these states effect the Scanning Tunneling Microscopy in a nonlinear manner. This subject will be the topic of Chapter 4. In this Chapter the results of electronic energy band calculation results will be given. The preliminary results of these study was reported before [56], where a different set of parameters was used and so there are some quantitative differences between them. However, the qualitative results are the same.

It is clear from the structure of the graphite that the interaction between the tip and the surface will be most significant when the tip atom is at the on-top position. At this position the internuclear distance between the tip and surface atoms is smallest for the given tip height. Furthermore, the symmetry of the original states allows localization of certain states. Therefore, the on-top position will be the focus of attention.

For several tip heights ranging from 1 $\overset{\circ}{A}$ to 5 $\overset{\circ}{A}$ the electronic band structure of the combined system is calculated by using the method described in Section 3.2.1. From the results three different regimes of interaction were identified.[2]

The first one is the chemical binding regime. This case occurs for tip heights between 1 $\overset{\circ}{A}$ and ~ 1.75 $\overset{\circ}{A}$. Both qualitative and quantitative features of states are changing drastically when one changes the height between these limits. The band diagrams for this interaction regime for four different tip heights are given in Figure 3.7. Some preliminary observations about the system is as follows:

i. The nearest-neighbor separation of graphite monolayer is ~ 1.45 $\overset{\circ}{A}$. Thus the cases under consideration correspond to chemical contact between the tip and the surface. For these tip heights the single atom approximation of

---

[2]The tip atom is taken to be on an A-type graphite monolayer atom. In spite of the fact that A- and B-type atoms are identical for a single layer, I will use this notation for the sake of brievity.

the tip is not very accurate since the interaction between the surface and the tip is large enough to effect the tip states very much alike the substrate states. Nevertheless, it gives an idea about the strong interaction of the tip and the surface.

ii. Due to the exponential scaling of interaction parameters, the rate of change of parameters is large as compared to that of the large tip heights. This variation may lead to changes in the band structure as well.

iii. The symmetry of this particular lateral position manifests the degeneracy of bands at some special points of Brillouin zone as explained in Section 3.1.1. In conjuction with (ii) one expects some important variation in the band structure as a function of tip height.

For the tip height equal to 1 Å (Figure 3.7.a):

- The bands labeled TS_1 are monolayer π-like states with a significant orbital contribution of B-type atoms. Around Γ point of the Brillouin zone the tip p_x and p_y states begin to mix with them. At Γ the energy is $-8.74 \ eV$ and the tip contribution is 17%.

- The band labeled T_1 is formed mainly by the tip p_z orbital and behaves like a bonding state of the tip and monolayer. The energy is $-8.10 \ eV$ without a significant dispersion, and the tip contribution is 85%.

- The bands labeled TS_2 are again mixed states of tip p_x and p_y orbitals and monolayer π^* and σ^* states. The contribution of the tip decreases towards
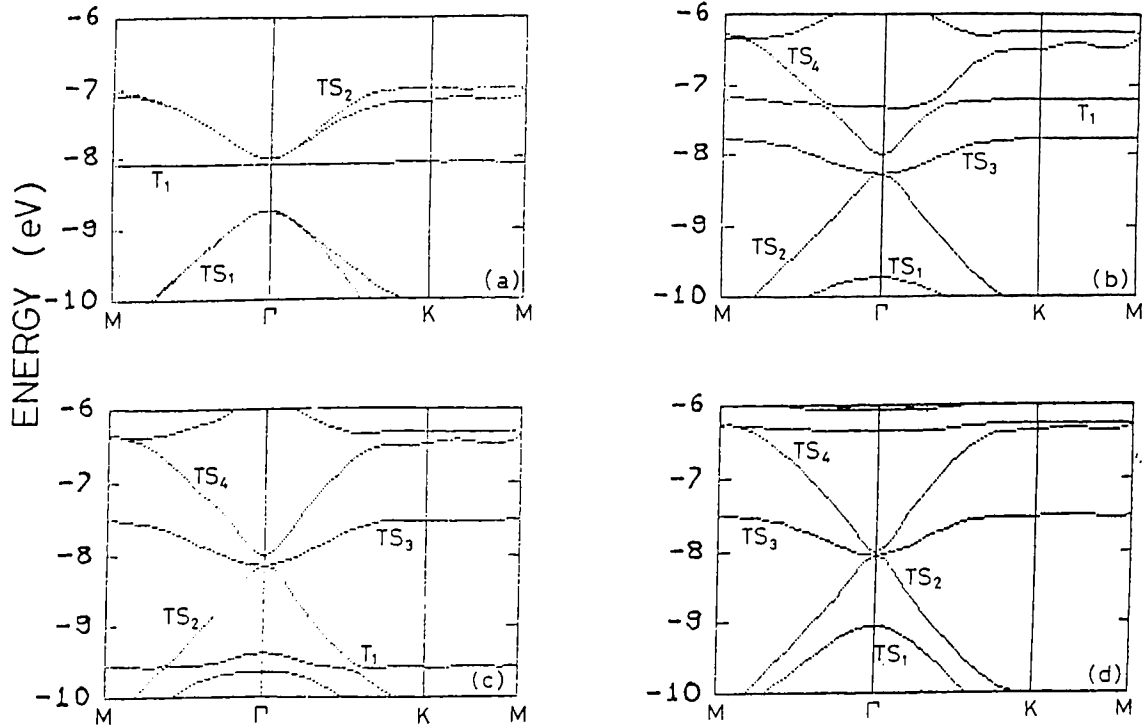
55

Figure 3.7: Band structure for the on-top position-I

Tip height is equal to a) 1.0 Å, b) 1.25 Å, c) 1.50 Å, d) 1.75 Å.

Γ point and diminishes there. At the Γ point the states are identically

monolayer states localized on the A-type atoms at $-8.0\ eV$ (E_F).

The earlier theories of Scanning Tunneling Microscopy of graphite were

based on the $m = 0$ orbitals of the tip[3], that is s and p_z for $l = 0$ and $l = 1$,

respectively [33]. The other orbitals which are elements of $m \neq 0$ classes

are shown to have minor effects on the tunneling current [34]. In the system

described above p_x and p_y orbitals play important roles. This is a direct result

of chemical bonding nature of the interaction. It will be shown that for larger

---

[3]m is the angular momentum component parallel to the z-axis. The $m \neq 0$ states have nodes
on the z-axis between the tip and the surface regions to result in smaller contributions to the
tunneling current.

tip heights, these states will not mix with others to contribute to the tunneling current appreciably. Thus, for those cases the result for non-interacting tip and surface model can be applied to the interacting model. At this point a comment about the validity of this calculation is in order. It is clear that a tip height of 1 $\mathring{A}$ is the chemical interaction regime, thus the fitted parameters in this Empirical Tight Binding method or the smooth pseudo-wavefunctions in a Pseudopotential calculation will be insufficient to represent the effects of the atomic cores which become effective for small distance. Nonetheless, these results can be used in a qualitative way, in order to explore the trend.

For the tip height equal to 1.25 $\mathring{A}$ (Figure 3.7.b):

- The bands labeled TS_1 in the previous case are not present for this tip height. The new band labeled TS_1 is a bonding state of the tip p_z orbital and π states of monolayer localized on the A-type atoms. Due to strong interaction it is well below the Fermi energy. At Γ, its energy is -9.73 eV and the tip contribution is rather small (3%).

- The band labeled TS_2 is reminescent of the above described bands for tip height 1 $\mathring{A}$ with an almost zero tip contribution. Its energy at Γ is -8.26 eV.

- The band labeled TS_3 is built up of both tip orbitals and monolayer π states localized on the B-type atoms. These states come together by a weak contribution of monolayer states of the A-type atoms. At Γ, the tip

contribution diminishes and the band becomes degenerate with TS_2. The tip contribution is mainly s-like and the rest from p_z.

- The band labeled T_1 is a bonding state of the tip s orbital and monolayer states. The tip contribution is 60% and the energy is $\sim -7.25\ eV$.

- The band labeled TS_4 is the reminiscent of the above described state TS_2 for 1 Å. The degeneracy is lifted and there is only one state with the same character. The tip contribution is smaller than that of TS_2 for 1 Å.

- Above these bands there are two bonding states of tip p_x and p_y orbitals and monolayer σ^* states. These bands are characteristic for the cases described below.

The change in the band structure shows a transition from the chemical binding to weak interaction between the tip and the surface. The energy of the tip s orbital and the symmetries of tip p_x and p_y orbitals imply the insignificant roles of these orbitals in Scanning Tunneling Microscopy. However, it should be noted that when the tip is extremely close to the surface the situation is no more tunneling but a chemical interaction. This leads to the formation of states originating from these orbitals and energies close to the Fermi level. However, when the tip retracts away from the surface the interaction becomes weaker. Due to the reduced interaction among the orbitals, the bands originated from these orbitals begin to shift to energies closer to the original orbital energies. The only relevant orbital, namely the tip p_z orbital, begins to contribute to the tip-surface mixed states in an essential way. The two diagrams for tip heights

of 1.5 Å and 1.75 Å show this shift of bands. The detailed analysis of these bands show that the main features are not very much different than the ones listed above for tip height of 1.25 Å. Therefore these band diagrams which are shown in Figure 3.7 .c and .d will not be analyzed in detail here.

The second regime apparent from the band diagrams is the weak interaction regime. This regime is named as *Tip Induced Localized States* regime. This regime includes tip heights from 2 Å to $\sim$ 3.5 Å. The band structures are shown in Figure 3.8. The qualitative features of the bands are the same for the whole range of tip heights. Only some quantitative properties are changing. This is why effects of tip height in Scanning Tunneling Microscopy are varying nonlinearly. The bands will be analyzed for tip height 2 Å in detail, and for other tip heights only the related quantities will be given.

For the tip height equal to 2 Å (Figure 3.8.a):

• The band labeled TS_1 is one of the Tip Induced Localized States. It is a mixture of the tip p_z orbital and the monolayer π states. The main contribution of monolayer is from the A-type atoms. Away from the Γ point the state has a small tip component and becomes a pure π state. At Γ it is a bonding state. To pictorize its local bonding character its local density of states is shown in Figure 3.9. The tip contribution increases towards the center of Brillouin zone. The energy at Γ is -8.63 eV, the tip contribution is 36%.
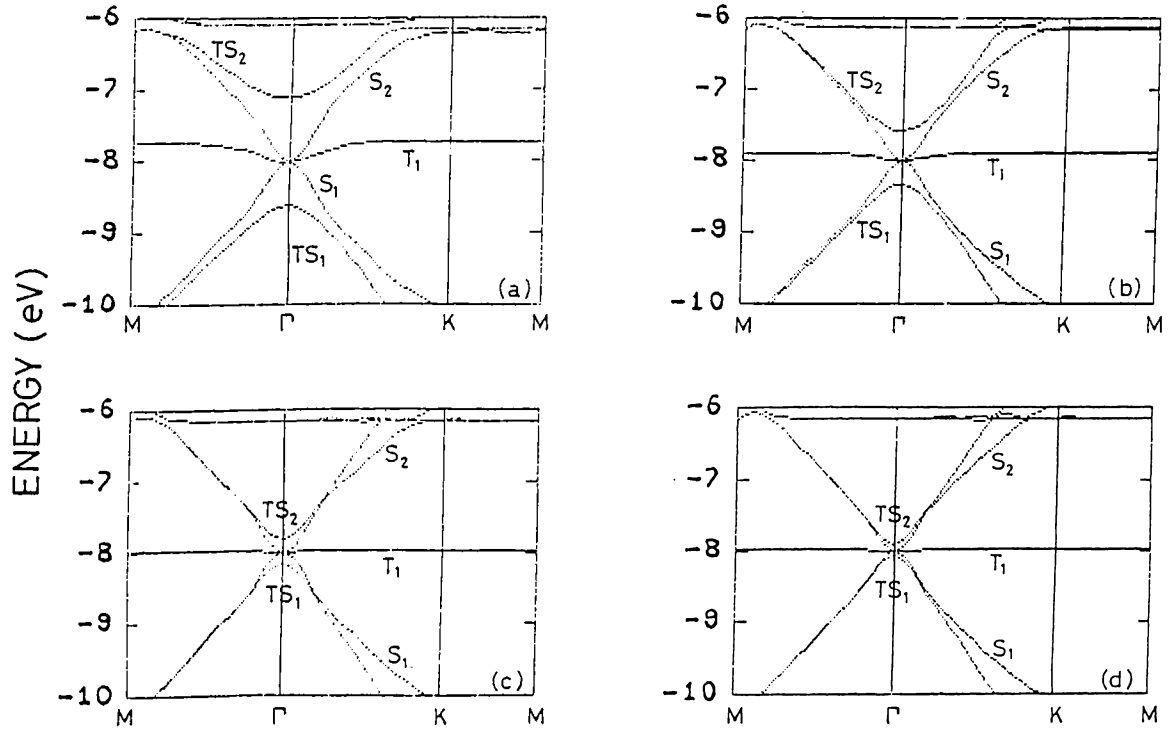
Figure 3.8: Band structure for the on-top position-II

Tip height is equal to a) 2.0 Å, b) 2.25 Å, c) 2.50 Å, d) 2.75 Å.

- The band labeled S_1 is almost like the free monolayer π state. The tip contribution is less than 1%. It is clear that this is a monolayer state which is both orthogonal to and not interacting with tip p_z orbital. Thus it survives without any change when the tip gets closer to the surface. At Γ it is exactly at the Fermi level.

- The band labeled T_1 has 75% tip p_z contribution away from Γ. The energy is -7.73 eV. Near the center of the Brillouin zone this band changes character and becomes a monolayer state. At Γ it is a pure monolayer state at the Fermi energy.

- The band labeled S_2 is the counterpart of S_1. It is a π^* state of the monolayer.

- The band labeled TS_2 is the counterpart of the first Tip Induced Localized State. It is produced by the tip p_z orbital and monolayer π^* state, and has anti-bonding character. At Γ, its energy is -7.12 eV and the tip contribution is %52.

- The states which have originated from the tip s, p_x and p_y orbitals are near the orbital energies of these states. Their monolayer contributions are very small. Due to the symmetry of Brillouin zone it is not possible to find doubly-degenerated states at a $\vec{k}$ point other than Γ or K. This leads to anti-crossing of bands. Around these anti-crossing points the tip and the monolayer states begin to mix. However this is not an essential interaction.

The detailed information about the tip height dependence of these quantities are given in Table 3.3. It is expected that the Tip Induced Localized States get closer to the Fermi energy with increasing tip height. This is a direct consequence of the decreasing strength of interaction. The third regime is just a smooth transition of Tip Induced Localized States into pure tip states. The numerical results do not fit to this expectation, but the reason for this is the degeneracy of the tip p_z orbital and monolayer state at the Fermi level for infinite separation. This point will be clearer with the discussion in Section 4.3. This full decoupling situation occurs at tip height ~ 3.5 $\mathring{A}$. Beyond this tip
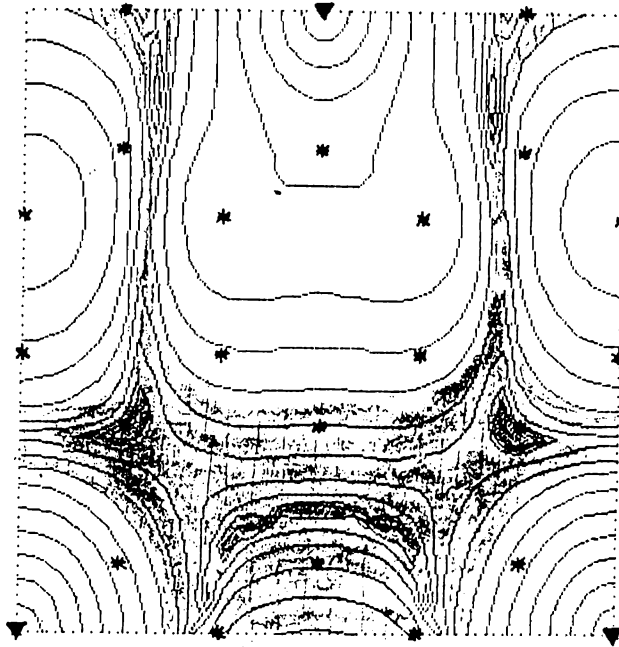
Figure 3.9: Local density of states for TS_1

The tip height is equal to 2.0 $\mathring{A}$. The density of states are calculated 2.0 $\mathring{A}$ above the monolayer. The dark areas represent the regions with low density. The density is changing by a factor 4.3 between two consecutive contours. Stars are the monolayer atom positions and triangles are the projections of the tip atoms on the monolayer plane.

height the band diagram of this total system is just projection of tip electronic energies onto the monolayer energy band. This regime is called the independent electrode regime.

This completes the discussion on the effects of the tip-surface interaction on the band structure of the system for the tip located at the on-top site position. As a final conclusion one can say that for small tip heights the independent electrode approximation fails and the system needs to be handled as a whole. This is the case for Scanning Tunneling Microscopy of graphite.

Table 3.3: The band results for the on-top position

tip height ($\mathring{A}$)	2.00	2.25	2.50	2.75	3.00
$E^{\Gamma}_{TS_1}$ (eV)	-8.63	-8.33	-8.17	-8.08	-8.04
tip contribution(%)	36	43	47	48	49
E_{T_1} (eV)	-7.73	-7.90	-7.97	-7.99	-8.00
tip contribution(%)	76	93	98	99	100
$E^{\Gamma}_{TS_2}$ (eV)	-7.12	-7.59	-7.81	-7.91	-7.96
tip contribution(%)	52	54	53	52	51

There are two other lateral positions of the tip which have importance as long as the effects of tip-surface interaction are concerned. One of them is the hollow site. This position is the center of the hexagonal honeycomb ring. The earlier theories predicted zero tunneling current for this position for a monolayer [50]. Now the band structures shown in Figure 3.10 will be analyze.

For the tip height equal to 1 $\mathring{A}$ (Figure 3.10.a):

- The bands labeled S_1 are monolayer π states. They deviated from the free monolayer bands in the vicinity of Γ. At this point the tip contribution is 7%, and the energy is -8.64 eV.

- The band labeled TS_1 is the binding state of the tip s and p_z orbitals and monolayer π states. The tip contribution is $\sim 90\%$ and at Γ the energy
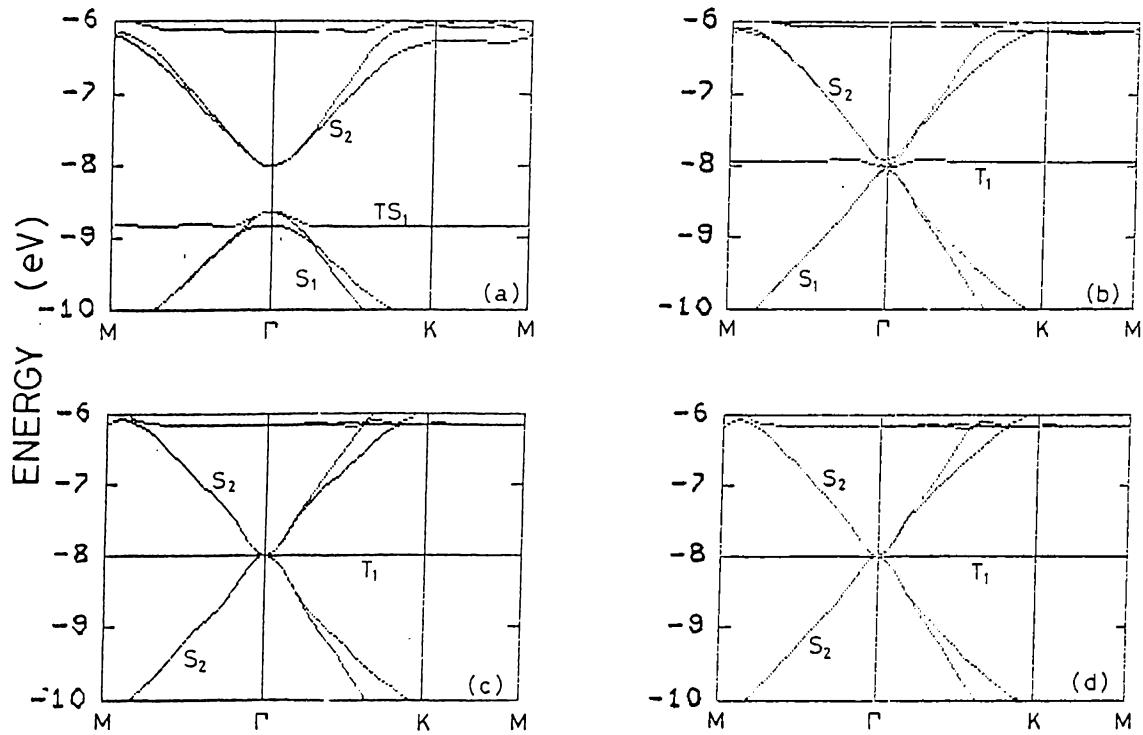
Figure 3.10: Band structure for the hollow-site position

Tip height is equal to a) 1.0 Å, b) 2.0 Å, c) 3.0 Å, d) 4.0 Å.

is -8.84 eV. There is an anti-crossing with S_1 bands near the center of Brillouin zone.

- The bands labeled S_2 are monolayer π^* states. The tip contribution is negligible. They are degenerate at the center of the Brillouin zone at the Fermi level.

The above observations show that for the hollow-site position there is a chemical bonding regime just as the on-top position. However, for this case the weak interaction regime is not important as it is for the previous one. The symmetry of hollow-site position predicts no bonding states at all. This is the

direct consequence of the equivalence of all six ring atoms, that is their phases for states at the Fermi level cancel each other to give a zero sum. Nevertheless for tip heights ~ 2 $\mathring{A}$, as a result of the long range interactions of the tip atom with the surface, one may find some pseudo-Tip Induced Localized States. For these states the tip contribution is still less than 2%. Thus one can conclude that no bonding states can be found for the hollow-site position. This remark is a stronger manifestation of a large corrugation for graphite in Scanning Tunneling Microscopy, as it will be explained in Chapter 4.

The third special position is the bridge position which lies at the middle of the line segment connecting two nearest-neighbors. The band structures are shown in Figure 3.11.

For the tip height equal to 1 $\mathring{A}$ (Figure 3.11.a):

- The bands labeled TS_1 and TS_2 are mixed states of the tip orbitals and the monolayer states. For TS_1 tip p_x and p_y contribution is $\sim 3\%$ and for TS_2 tip s and p_z contribution is $\sim 7\%$. Their energies are ~ -9.2 eV and -7.2 eV, respectively. The anti-crossings with other bands are clearly visible.

- The bands labeled S_1 and S_2 are mainly monolayer π and π^* states. The tip contribution is less than 3%. They are degenerated at the center of Brillouin zone with energies at the Fermi level.
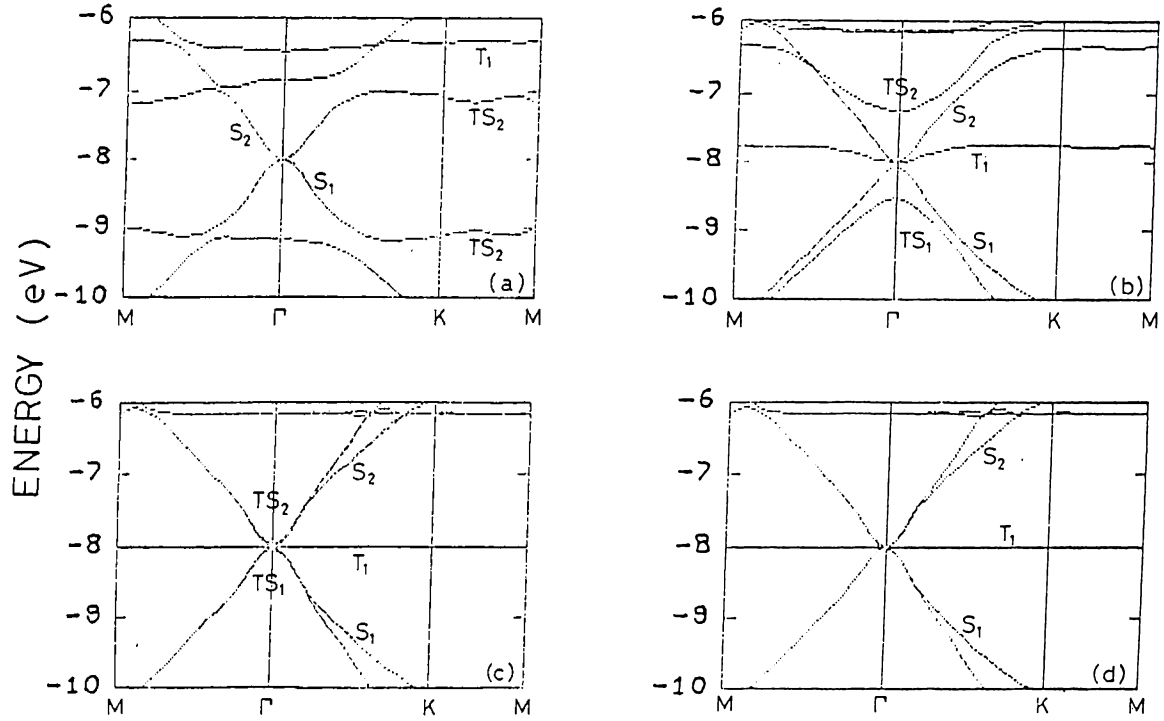
65

Figure 3.11: Band structure for the bridge position

Tip height is equal to a) 1.0 Å, b) 2.0 Å, c) 3.0 Å, d) 4.0 Å.

- The band labeled T_1 is a tip p_x and p_y band at energy -6.3 eV. Again the anti-crossings are tractable.

This case again exhibits the basic features of chemical binding. Due to the geometry and the symmetry of bridge position the weak interaction regime is not as effective as it was for the on-top position. The bands shown in Figure 3.11.b and .c are qualitatively equivalent to those in Figure 3.8. The quantitative results are given in Table 3.4.

The above analysis shows that the tip-surface interaction at the atomic

Table 3.4: The band results for the bridge position

tip height ($\mathring{A}$)	2.00	3.00
$E_{TS_1}^{\Gamma}$ (eV)	-8.53	-8.04
tip contribution(%)	37	49
E_{T_1} (eV)	-7.77	-8.00
tip contribution(%)	81	100
$E_{TS_2}^{\Gamma}$ (eV)	-7.23	-7.96
tip contribution(%)	55	51

scale is playing a dominant role in electronic band structure for small tip heights. It is expected that the tunneling phenomenon will be modified as a result of the presence of these Tip Induced Localized States. This will be the subject of Chapter 4.

Chapter 4

Tunneling Current for Small Tip Height Regime

4.1 Bardeen's Formalism for Tunneling

In Section 2.3 it was pointed out that the theory used for the Scanning Tunneling Microscopy is based on Bardeen's formalism [11] for tunneling. In the present section this formalism and its application to Scanning Tunneling Microscopy will be outlined.

The phenomenon of tunneling is a transition between two states which are originally eigenstates of different structures. This transition is activated by the overlap of the wavefunctions in the region which separates those structures, the so-called barrier region. The preceding brief description can be taken as the starting point of Bardeen's formalism [11]. It is very appropriate to expand the total wavefunction for tunneling in terms of the original eigenstates of two electrodes, so that for $t \to -\infty$ this state will be approximately equal to one of left electrode's eigentstates, and for $t \to \infty$ there will be transmitted and

reflected constituents of the total wavefunction.

In Bardeen's theory electrons are treated in one-dimension, but by a careful analysis the theory can be extended to three-dimension. The tunneling structure that he had used in his original work is a barrier region extending between x_a and x_b ($x_a < x_b$) and two semi-infinite electrodes. Since one of the most important cases of tunneling is with superconducting electrodes, he employs a many-particle description of the electrodes. This many-body form can be simplified to give a one-particle expression for Scanning Tunneling Microscopy studies, since the many-body aspects of this phenomenon is not known completely, and the systems that are investigated can be analyzed by an effective one-particle Hamiltonian without considerable errors.

For the system described above let us consider the ground state Ψ_0 and an excited state Ψ_{mn} which differs from the former by the transfer of a quasi-electron labeled m from the left electrode into a quasi-electron state n in the right electrode. The quasi-particle concept is used to emphasize that these states are many-body states. These quasi-electron states m and n are oscillatory in the left and right electrodes, respectively, and decaying exponentially into the barrier region. Bardeen assumed that these wavefunctions smoothly approach to zero beyond the edge of the barrier, into the other electrode [11]. Thus these states are the quasi-particle states of infinitely separated electrodes in the first order.

69

some given regions of space. The same method that is used for the decay of a state into others can also be used here. Since the electron is initially in Ψ_0 and assuming that $da_0/dt \simeq 0$, $b_{mn}(t) \simeq 0$, and $a_0(t) \simeq 1$, one finds a simple expression for the transition amplitude from Ψ_0 to Ψ_{mn}, that is for the tunneling from the left to the right electrode.

$$i\hbar \dot{b}_{mn}(t) \simeq\, < \Psi_{mn} \mid \mathbf{H} - E_0 \mid \Psi_0 >\, e^{-i(E_0 - E_{mn})t/\hbar} \qquad (4.5)$$

Because the prefactor of the exponential does not depend on time, one gets a Dirac-delta function after the time integration. The total tunneling probability is given by the magnitude squared of the total transition amplitude. The possibility of degeneracy is excluded here by using a quasi-continuous spectrum for the electrodes, then the resulting probability will be the sum of individual probabilities due to the Dirac-delta functions. Finally, the tunneling current can be written as:

$$\mathbf{I}_t = \frac{2\,\pi\,e}{\hbar}\, \sum_{mn} \mid M_{mn} \mid^2\, \delta(E_0 - E_{mn}) \qquad (4.6)$$

where, $M_{mn} =\, < \Psi_{mn} \mid \mathbf{H} - E_0 \mid \Psi_0 >$. Note that the tunneling current can be written as the product of the electronic charge and the transition probability per unit time. This final form is very similar to the Fermi's Golden rule in time-dependent perturbation theory.

The specifics of the tunneling problem enables one to simplify the expression for M_{mn}. From Equation 4.1 it is clear that the integral for M_{mn} is over $\mathcal{R}_R$ only, since in $\mathcal{R}_L$ the integrand is identically zero. To make the integral

71

symmetric in L and R one can add a term which vanishes identically in $\mathcal{R}_R$ [11]. Using Equation 4.1 one gets:

$$M_{mn} = \int_{\mathcal{R}_R} d^3r \ [\Psi_{mn}^*(\mathbf{H} - E_0)\Psi_0 - \Psi_0(\mathbf{H} - E_{mn})\Psi_{mn}^*] \qquad (4.7)$$

The total Hamiltonian consists of a part including the kinetic terms, and the potential energy part. The potential energy part does not contribute to the above integral. The expression then simplifies to:

$$M_{mn} = \frac{-\hbar^2}{2\,m} \int_{\mathcal{R}_R} d^3r \ [\Psi_{mn}^* \nabla^2 \Psi_0 - \Psi_0 \nabla^2 \Psi_{mn}^*] \qquad (4.8)$$

where $-\hbar^2/2m \ \nabla^2$ is used for the summation of kinetic energy operators of all electrons in the system. Using Gauss' law one finds:

$$M_{mn} = \frac{-\hbar^2}{2\,m} \int_{\partial \mathcal{R}_R} d\vec{S} \cdot [\Psi_{mn}^* \vec{\nabla} \Psi_0 - \Psi_0 \vec{\nabla} \Psi_{mn}^*] \qquad (4.9)$$

where $d\vec{S}$ is the infinitesimal normal vector pointing towards $\mathcal{R}_L$ and the integration is over the boundary of $\mathcal{R}_R$. The integrand has a similar form as the quantum mechanical current operator. As before, the difference lies in the fact that these states form an overcomplete non-orthogonal basis. Bardeen defined the current operator as [11]:

$$M_{mn} = -i \ \hbar \ \int_{\partial \mathcal{R}_R} d\vec{S} \cdot \vec{J}_{mn} \qquad (4.10)$$

where:

$$\vec{J}_{mn} = \frac{1}{i\,2\,\hbar\,m}[\Psi_{mn}^* \vec{\nabla} \Psi_0 - \Psi_0 \vec{\nabla} \Psi_{mn}^*] \qquad (4.11)$$

In the one-dimensional case this current density is constant in the interval $[x_a, x_b]$ irrespective of the actual point of evaluation and the integral in

Equation 4.9 can be computed over any surface lying within $\mathcal{R}_R \cap \mathcal{R}_L$. This final current expression is used in most of Scanning Tunneling Microscopy studies by replacing many-body wavefunctions with effective one-particle wavefunctions, due to the assumption of only one particle involves in tunneling, and adding the bias term. In order to include the statistical probabilities of individual transitions, appropriate Fermi-Dirac distribution functions are also included:

$$\mathbf{I}_t = \frac{2\,\pi\,e}{\hbar} \sum_{\alpha\beta} \mid M_{\alpha\beta} \mid^2 \delta(E_\alpha - E_\beta + eV)\, f(E_\alpha + eV)\, [1 - f(E_\beta)] \qquad (4.12)$$

where α labels the tip states and β the states of the sample, f is the Fermi-Dirac distribution, and V is the bias applied between the tip and the sample.

Bardeen's expression is not adequate for analyzing the effects of Tip Induced Localized States in Scanning Tunneling Microscopy, and has to be modified accordingly. In the next Section this modification will be handled.

4.2 Tunneling Current in the Presence of Tip Induced Localized States

Bardeen's approach to the tunneling, described in the preceding Section, originates from the assumption that the tunneling phenomenon can be described in terms of original eigenstates of two electrodes. As it is discussed in detail in Section 3.2.2 when the tip height becomes of the order of nearest-neighbor spacing of the surface under consideration some Tip Induced Localized States

begin to be formed in the vicinity of the tip. It is shown that these states effect the electronic band structure of the system in an essential manner. Consequently one expects them to have their effects in the tunneling current as well.

The first observation is that for the above outlined system, the previously used theory becomes insufficient. In Bardeen's formalism [11] for a new set of physically different states, that is for the states of the second electrode, the set of basis functions was added to the previous one at the cost of overcompleteness. Using this argument, I included a new set of states, namely the Tip Induced Localized States in the basis set used by Bardeen. It is clear that the original basis set is sufficient to express these states, nonetheless in order to display the physical implications of these new localized states it is necessary to include them explicitly.

The second observation is about the physical meaning of Bardeen's current expression. If the total Hamiltonian **H** of the system could be solved, the tunneling current can be expressed in terms of the eigenstates of this single Hamiltonian. This is the case for one-dimension for which the barrier profile becomes a simple analytic expression, such as of rectangular or trapezoidal shapes. Those solutions can be used in the simple quantum mechanical current expression in order to find the total current. The analysis of Chapter 3 is not to be confused with this type of a calculation. For a complete analysis of the

system, emphasis should be given also to the extended nature of the electrodes in addition to the local effects. The Empirical Tight Binding calculations used in this study includes only the local interaction of the tip and the surface, but not their extended natures. Therefore, results of the electronic structure calculations have to be used in conjuction with the traveling wave solutions of the electrodes to get a correct expression for tunneling current.

In the new scheme, the space is divided to three fictitious regions. In addition to Bardeen's left and right regions I use a new region $\mathcal{R}_{TILS}$ which lies in the close proximity of the tip, and where the Tip Induced Localized States are good solutions of the total Hamiltonian.

$$
\begin{array}{rcll}
\mathbf{H}\ \Psi_{tip}(\vec{r}) & = & E_{tip}\ \Psi_{tip}(\vec{r}) & \vec{r} \in \mathcal{R}_{tip} \\
\mathbf{H}\ \Psi_{s}(\vec{r}) & = & E_{s}\ \Psi_{s}(\vec{r}) & \vec{r} \in \mathcal{R}_{s} \\
\mathbf{H}\ \Psi_{TILS}(\vec{r}) & = & E_{TILS}\ \Psi_{TILS}(\vec{r}) & \vec{r} \in \mathcal{R}_{TILS}
\end{array} \tag{4.13}
$$

where s stands for R in Equation 4.1, and tip for L. The total wavefunction is now constructed by including these new states , similar to Equation 4.3. Using the approximations $b_{TILS}, b_s \simeq 0;\ da_{tip}/dt \simeq 0;$ and $a_{tip} \simeq 1$ the Schrödinger equation leads to the following set:

$$
\left[\begin{array}{c} \dot{b}_s \\ \dot{b}_{TILS} \end{array} \right] = \frac{-i}{\hbar\,(1-\mid S \mid^2)} \left[\begin{array}{c} (M_{s-tip} - S^*\ M_{TILS-tip})\ e^{-i(E_{tip}-E_s)t/\hbar} \\ (M_{TILS-tip} - S\ M_{s-tip})\ e^{-i(E_{tip}-E_{TILS})t/\hbar} \end{array} \right] \tag{4.14}
$$

where:

$$
\begin{array}{rcl}
S & = & \int d^3r\,\Psi^*_{TILS}\Psi_s \\
M_{s-tip} & = & \frac{-\hbar^2}{2\,m}\ \int d\vec{S}\cdot(\Psi^*_s\vec{\nabla}\Psi_{tip} - \Psi_{tip}\vec{\nabla}\Psi^*_s) \\
M_{TILS-tip} & = & \frac{-\hbar^2}{2\,m}\ \int d\vec{S}\cdot(\Psi^*_{TILS}\vec{\nabla}\Psi_{tip} - \Psi_{tip}\vec{\nabla}\Psi^*_{TILS})
\end{array} \tag{4.15}
$$

75

where the integrations are over the boundary of $\mathcal{R}_{tip}$. Carrying out the integrations one gets:

$$I = \frac{2\,\pi\,e}{\hbar\,(1-\mid S \mid^2)^2} \sum_{s,tip} \mid M_{s-tip} - S^*\,M_{TILS-tip} \mid^2\ \delta(E_{tip} - E_s) \qquad (4.16)$$

This expression is the final form that can be obtained at this point. Some approximations may cause it to simplify into a more compact form. These cases will be investigated in Section 4.4 and 4.3.

4.3 A Simple Model for the Effects of Tip-Surface Interaction

The derivation of the tunneling current in Section 4.2 showed that as a result of the tip-surface interaction the tunneling states of the combined system are different from a simple superposition of the original states of two electrodes. As a simple picture of this result, here the problem for the on-site position of graphite will be analyzed.

The atomic structure for the tip at the on-top position was investigated in Section 3.1.1. The relevant basis states for the system are the p_z orbital of the tip φ_{tip}, and the Fermi level states of the surface φ_I, φ_I^*, φ_{II}, and φ_{II}^*. Where φ_I and φ_I^* are two linearly independent states localized on the A-sublattice and at the Fermi level, and φ_{II} and φ_{II}^* are the same for the B-sublattice. The Tip Induced Localized States can be expressed in terms of these basis states as a

76

first order approximation. The problem reduces to finding the eigenstates of the combined system:

$$\Psi = \sum_i a_i \, \varphi_i \qquad i = \text{tip}, \text{I}, \text{I*}, \text{II}, \text{II*} \qquad (4.17)$$

$$\mathbf{H} \, \mathbf{a} = E\mathbf{a} \qquad (4.18)$$

It is clear that the basis states φ_{II} and φ_{II}^* do not have any non-zero matrix elements with other basis states. Thus the final Hamiltonian matrix is as follows:

$$\mathbf{H} = \begin{bmatrix} E_{tip} & H_{t-I} & H_{t-I} \\ H_{t-I} & E_I & 0 \\ H_{t-I} & 0 & E_I \end{bmatrix} \qquad (4.19)$$

Here the fact that the H_{t-I} is real, is due to the strong short-range interaction between the tip and the surface. The system is assumed to be in the Tip Induced States regime, thus only the nearest-neighbor interactions are considered. Note that $E_I = E_{II} = E_F$. Another observation is the symmetry for φ_I and φ_I^*. The three eigenstates of the system are obtained as:

$$
\begin{aligned}
E &= E_F & \Psi &= \varphi_{II} \\
E &= E_F & \Psi &= \varphi_{II}^* \\
E &= E_F & \Psi &= \frac{\varphi_I - \varphi_I^*}{\sqrt{2}}
\end{aligned}
\qquad (4.20)
$$

The presence of these undistorted states was seen in Section 3.2.2 as well. In order to find the Tip Induced Localized States one has to solve the following 2×2 matrix equation in terms of φ_{tip} and $(\varphi_I + \varphi_I^*)/\sqrt{2}$:

$$\begin{bmatrix} E_{tip} & \sqrt{2}\, H_{t-I} \\ \sqrt{2}\, H_{t-I} & E_I \end{bmatrix} \begin{bmatrix} a_{tip} \\ a_{I+} \end{bmatrix} = E \begin{bmatrix} a_{tip} \\ a_{I+} \end{bmatrix} \qquad (4.21)$$

The solutions are:

$$E_{1,2} = \frac{E_I + E_{tip}}{2} \pm \left[\left(\frac{E_I - E_{tip}}{2}\right)^2 + 2\, H_{t-I}^2 \right]^{1/2} \qquad (4.22)$$

77

At this point certain realistic considerations are in order. The tip is assumed to be at a infinitesimally higher energy than the surface in order to guarantee that there will be a tunneling current from the tip to the surface. The interaction of the tip and the surface is an exponentially decaying function of the distance. That is one takes:

$$\begin{aligned} E_{tip} &= E_F + q\ V_0 \\ H_{t-I} &= q\ U_0\ e^{-\mu h} \end{aligned} \tag{4.23}$$

where q is the electronic charge and h is the tip height. Substituting these in Equation 4.22 one gets:

$$E_{1,2} = E_F + \frac{qV_0}{2} \pm q\ U_0 e^{-\mu h} \left[e^{2\mu h}(\frac{V_0}{2\ U_0})^2 + 2 \right]^{1/2} \tag{4.24}$$

$$a_{I+}^{(1,2)} = -e^{\mu h}\left\{ \frac{V_0}{4\ U_0} \mp \frac{1}{2} \left[(\frac{V_0}{2\ U_0})^2 + 2\ e^{-2\mu h} \right]^{1/2} \right\}\ a_{tip}^{(1,2)} \tag{4.25}$$

It is clear that E_1 corresponds to the anti-bonding state, and E_2 corresponds to the bonding state. One important limiting case is the independent tip regime, namely $h \rightarrow \infty$. In this limit both of the energies approach to the Fermi level.

$$\begin{aligned} a_{I+}^1 &= 0 \\ a_{tip}^2 &= 0 \end{aligned} \tag{4.26}$$

Thus the tip and surface states decouples. The bias is assumed to be low enough for the tip heights of interest, so that one can write:

$$\begin{aligned} a_{I+}^{(1,2)} &= \mp \frac{1}{\sqrt{2}}\ a_{tip}^{(1,2)} = \mp \frac{1}{2} \\ E_{1,2} &= E_F \pm \sqrt{2}\ q\ e^{-\mu h} U_0 \end{aligned} \tag{4.27}$$

Now using these results in Equation 4.16 one obtains the tunneling current. Note that the overlap of the Tip Induced State and the original monolayer state is:

$$S = \sqrt{2}\ a_{I+} = \frac{1}{\sqrt{2}} \tag{4.28}$$

78

There is a point which needs special attention. For the independent electrode regime S becomes one and the current becomes infinite. However it follows from the discussion of Section 4.2 that the related Tip Induced States have to be empty prior to tunneling. On the contrary the bonding state is filled and contributes only to the higher order effects which are neglected in Bardeen's formalism. Therefore one gets for $V_0 \ll U_0 e^{-\mu h}$ by using the normalization of the states and the simple phases of the terms in the magnitude square bracket in Equation 4.16:

$$I = 4 \frac{2\,\pi\,q}{\hbar} \sum_{s,tip} \mid M_{s-tip} - \frac{M_{TILS-tip}}{\sqrt{2}} \mid^2 \; \delta(E_{tip} - E_F) \qquad (4.29)$$

The matrix elements M can be calculated by considering the original problem. Since the self-consistent corrections are neglected, the M's are the ones which will appear in the equations for the independent tip regime. That is it is sufficient to use the Tip Induced Localized State and the original states of the electrodes to calculate the matrix elements above. One writes:

$$\sum_{s,tip} M_{s-tip} = (\frac{\hbar}{2\,\pi\,q}\,I_{LDOS})^{1/2} \qquad (4.30)$$

$$\sum_{s,tip} M_{TILS-tip} = -i\,(\frac{\hbar}{2\,\pi\,q}\,I_{TILS-tip})^{1/2} \qquad (4.31)$$

where I_{LDOS} is the current calculated in the independent electrode approximation, and $I_{TILS-tip}$ is the current input into the Tip Induced Localized State from the tip:

$$I_{TILS-tip} = \frac{q\,\hbar\,k_F}{m} \mid c_t \mid^2 \qquad (4.32)$$

where k_F is the Fermi wave-vector and c_t is the tip contribution to the Tip

79

Induced Localized State and is given by:

$$c_t = a_{tip} = \frac{1}{\sqrt{2}} \qquad (4.33)$$

The final form of the current expression becomes:

$$I = \{4 \ I_{LDOS} + 2 \ I_{TILS-tip}\} = (4 \ I_{LDOS} + G \mid c_t \mid^2) \qquad (4.34)$$

where G includes only geometrical terms and material parameters, and is of the order of I_{LDOS}. Note that Equation 4.34 is valid for on-top site only. As a first-order approximation G is the ratio of the exponential factors of tip and surface wavefunctions, that is $G/I_{LDOS} = k_F/\kappa$ and for typical experimental values is equal to 1.25. Thus at the on-top position the real current is ~ 5.25 times larger than the one calculated by using the independent electrode approximation.

As it was shown in Section 3.2.2 for the hollow-site position of the tip no Tip Induced Localized States exist. Therefore the independent electrode approximation is valid for small tip heights as well. The current is simply I_{LDOS}.

It is clear that the Tip Induced Localized States affect the tunneling in an essential way. For a general position of the tip it is hard to obtain an analytical calculation for the resulting current, as done in this Section. In the following Section the results for the graphite surface will be given.

4.4 Tunneling Current For Small Tip Heights: Graphite

The analytical model of the previous Section showed that there can be large enhancements in tunneling current as a result of the tip-surface interaction. To observe these effects I carried out numerical calculations using the methods described in Section 3.2.1 for tip heights ranging from 2 Å to 2.75 Å. In Section 3.2.2 it is shown that in this range the electronic structure belongs to the Tip Induced Localized States regime. For the other two regimes described there, there is no need for extensive analysis of current. In the chemical binding regime the tip and the surface are electrically connected to each other and this is not a normal operation mode of the Scanning Tunneling Microscope. In the independent electrode regime, previous theories give acceptable results in terms of the local density of states at the Fermi level. In this Section the results of these calculations will be presented.

Before analyzing the results of the combined system, it will be beneficial to look at the independent electrode approximation results. The local densities of states at Fermi level are shown in Figure 4.1. In Figure 4.2 the same quantity is shown as a function of both height from the surface and the lateral position. It is clear from the figure that, the corrugation of the local density gets smaller as one gets away from the surface. This remark is in disagreement with Tersoff's result [50]. But his six-plane-wave expansion is just an approximation
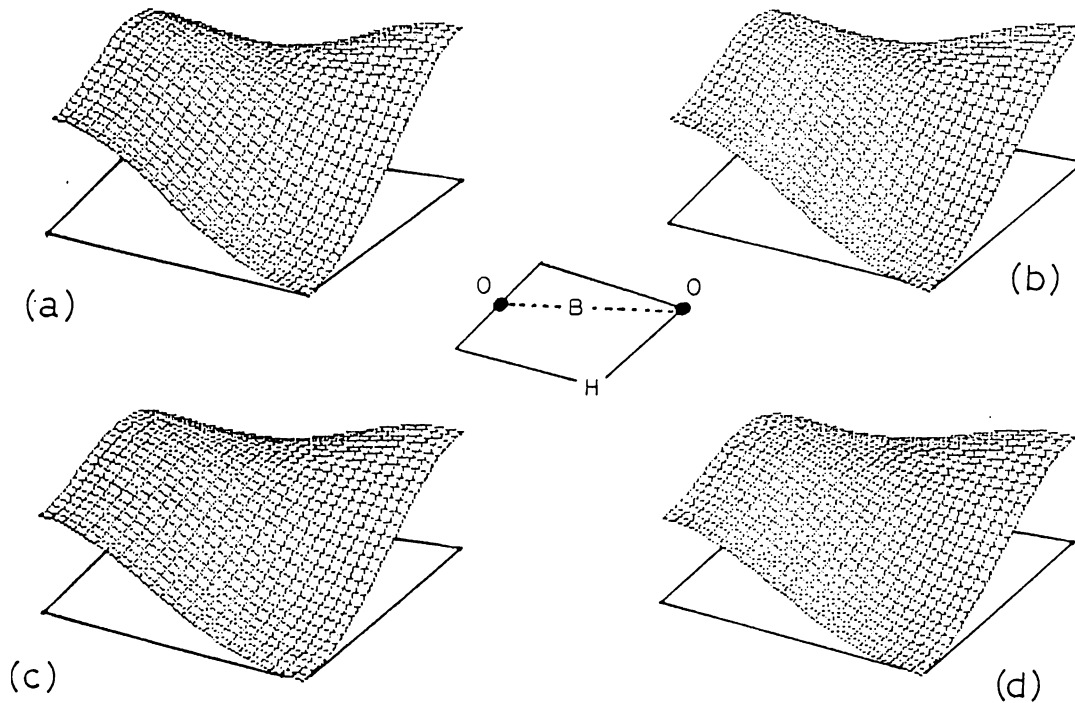
Figure 4.1: Local density of states for graphite monolayer

Tip height is a) 2.0 Å, b) 2.25 Å, c) 2.5 Å, d) 2.75 Å. The inset shows the geometry of the cell in which the corresponding quantities are calculated. O stands for the on-top site, H for the hollow site, and B for the bridge site.

to the realistic model, and does not contain wavevectors other than the smallest reciprocal lattice vectors, which are responsible for the local features of the state function and the smoothening of the density at large distances.

In the absence of the tip-surface interaction these functions would determine the tunneling current. However there are also the Tip Induced Localized States. Their energies as a function of tip height and lateral position are shown in Figure 4.3. It is observable that the effect of interaction is
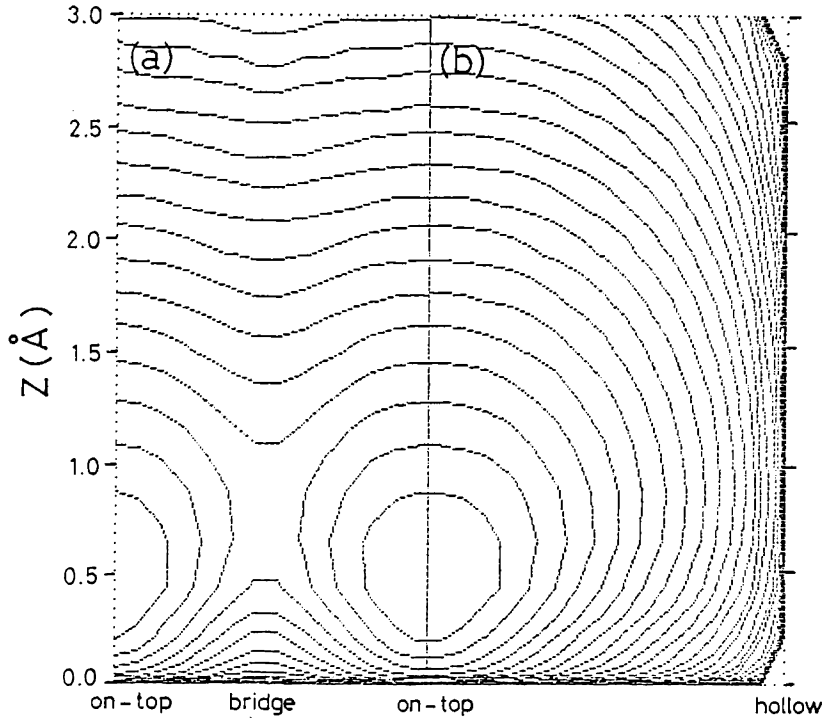
Figure 4.2: Local density of states in the vertical plane for graphite monolayer

a) Along the line between two on-top sites, b) Along the line between an on-top site and a hollow-site. The density is changing by a factor 1.65 between two consecutive contours

maximum at the on-top position and diminishes smoothly towards the hollow-site position. To compare these results of the Empirical Tight Binding method with the results obtained by the analytical method described in the previous Section, Tip Induced Localized State energies for the on-top position and different heights are shown in Figure 4.4. This curve is fitted to an exponential function and the following parameters for that are found:

$$\mu = 3.06 \; \overset{\circ}{A}{}^{-1} = 1.59 \; a.u.{}^{-1} \tag{4.35}$$

$$qU_0 = 11.04 \; eV \tag{4.36}$$

These values are very close to the ones used in the numerical band
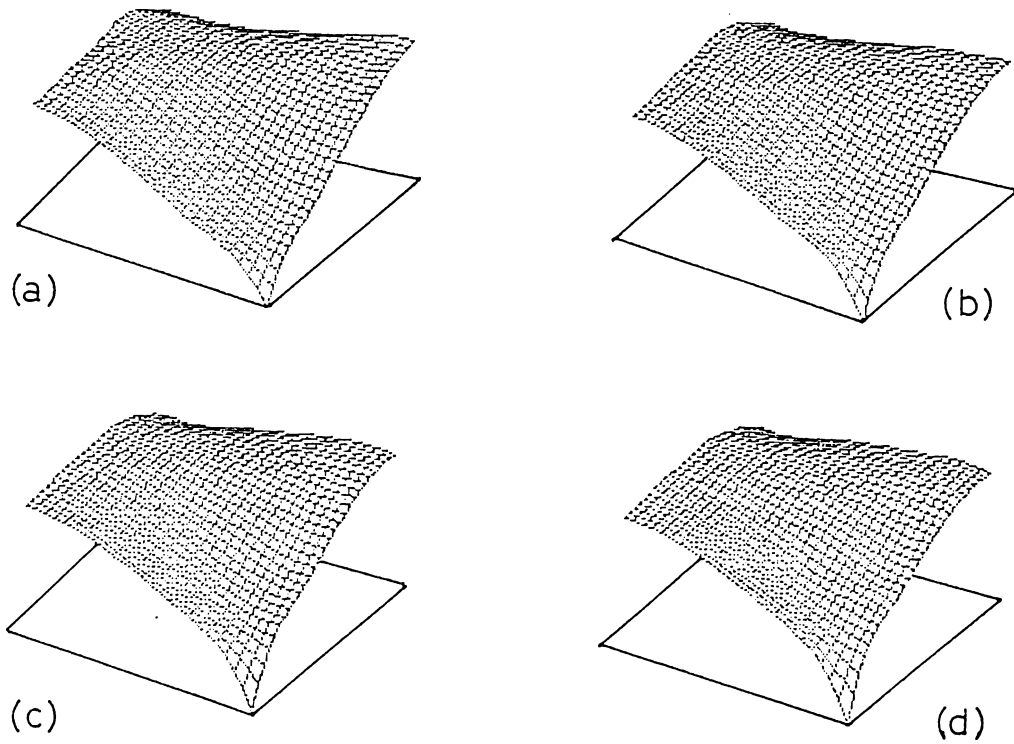
Figure 4.3: Energies of tip induced localized states

Tip height is a) 2.25 Å, b) 2.5 Å, c) 2.75 Å, d) 2.75 Å. The geometry is the same as Figure 4.1.

calculations, namely to 1.5888 and 9.4846, respectively. The error in U_0 is due to the shift of the tip p_z state to higher energy, thus the related shift of this state with respect to its original energy level. Thus the Tip Induced Localized State regime is confirmed once more.

The calculations reveal that at any position of the unit cell, except the hollow-site position, Tip Induced Localized States are formed. Furthermore the tip contribution to these states are almost equal at all of these points. This can be understood as a consequence of the degeneracy of the tip and the surface
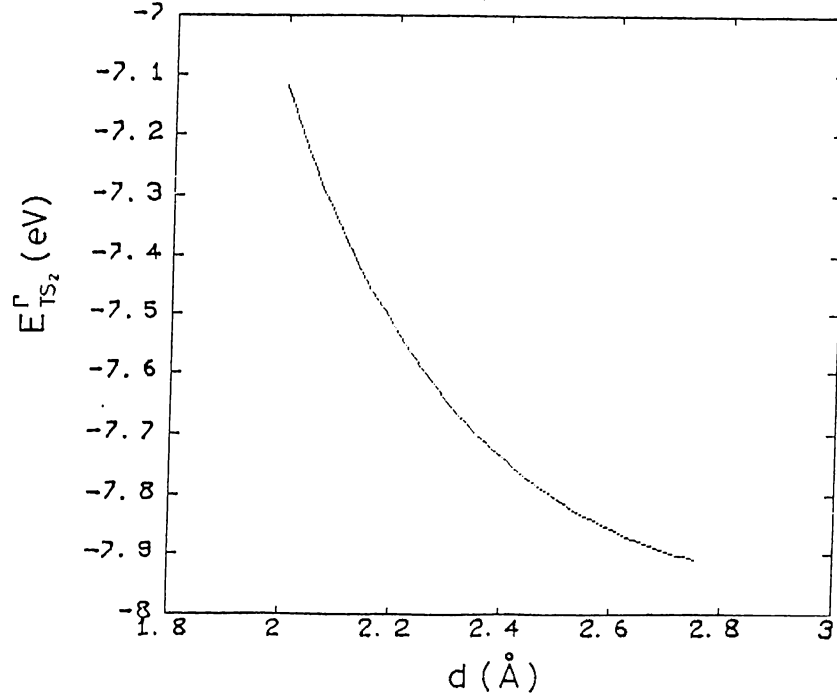
Figure 4.4: Energies of tip induced localized states: On-Top Position

states. This degeneracy is lifted when the small bias is of the same order as the

tip-surface interaction parameter:

$$V_0 \sim U_0 \ e^{-\mu h} \tag{4.37}$$

for a bias of 10 mV, the relevant distance is ~ 3.5 Å. The tunneling is modified

by the presence of the Tip Induced Localized States when the tip height is

smaller than this value.

It is shown in Section 3.2.2 that there are three undistorted Fermi level

states even in the presence of the Tip Induced Localized States. Thus in the

four dimensional basis space formed by φ_I, φ_I^*, φ_{II}, and φ_{II}^* the tip determines

one direction and there are three states produced by the monolayer states, and

at the Fermi level. In order to find S to be used in Equation 4.16 one just takes
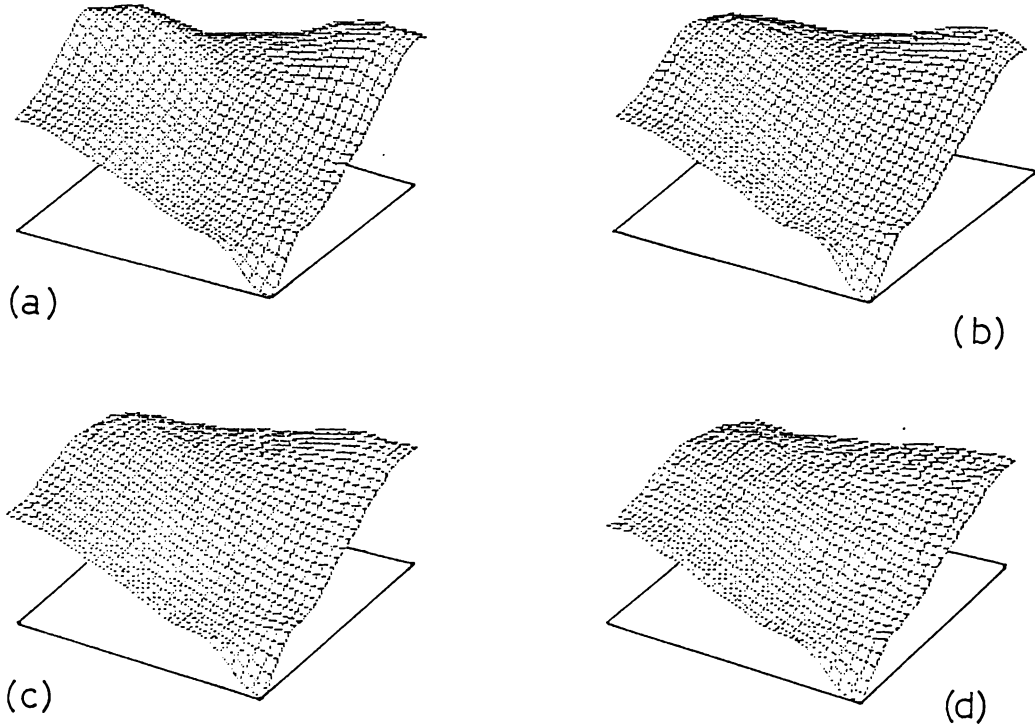
85

Figure 4.5: Tunneling current

Tip height is a) 2.25 Å, b) 2.5 Å, c) 2.75 Å, d) 2.75 Å. The geometry is the same as
Figure 4.1.

the square of the magnitude of this value. One can use the relation:

$$I = \{1- \mid S \mid^2\}^{-2}(I_{LDOS}+ \mid S \mid^2 G \mid c_t \mid^2) \tag{4.38}$$

for calculating the tunneling current for any tip position. Now remains the
determination of G. From the definition of M_{TILS-t} it is clear that the relevant
integration is over the boundary of the tip region, $\mathcal{R}_{tip}$. Thus G corresponds to
a transition probability from the tip into the Tip Induced Localized State. It
is more like a real current, however as the tip height increases it gets smaller
as result of localization near electrodes. Therefore it is a good approximation

to use a scaling procedure for G according to the height of the tip. I scaled G by the on-top site current, by using the approximate form given in Section 4.3. The results for the tunneling current is shown in Figure 4.5.

The tunneling current is shown in Figure 4.6 to emphasize the enhancement due to the presence of the Tip Induced Localized States. The current is traced for a tip height of 2.25 Å and along the line connecting the on-top site to hollow-site and bridge site.
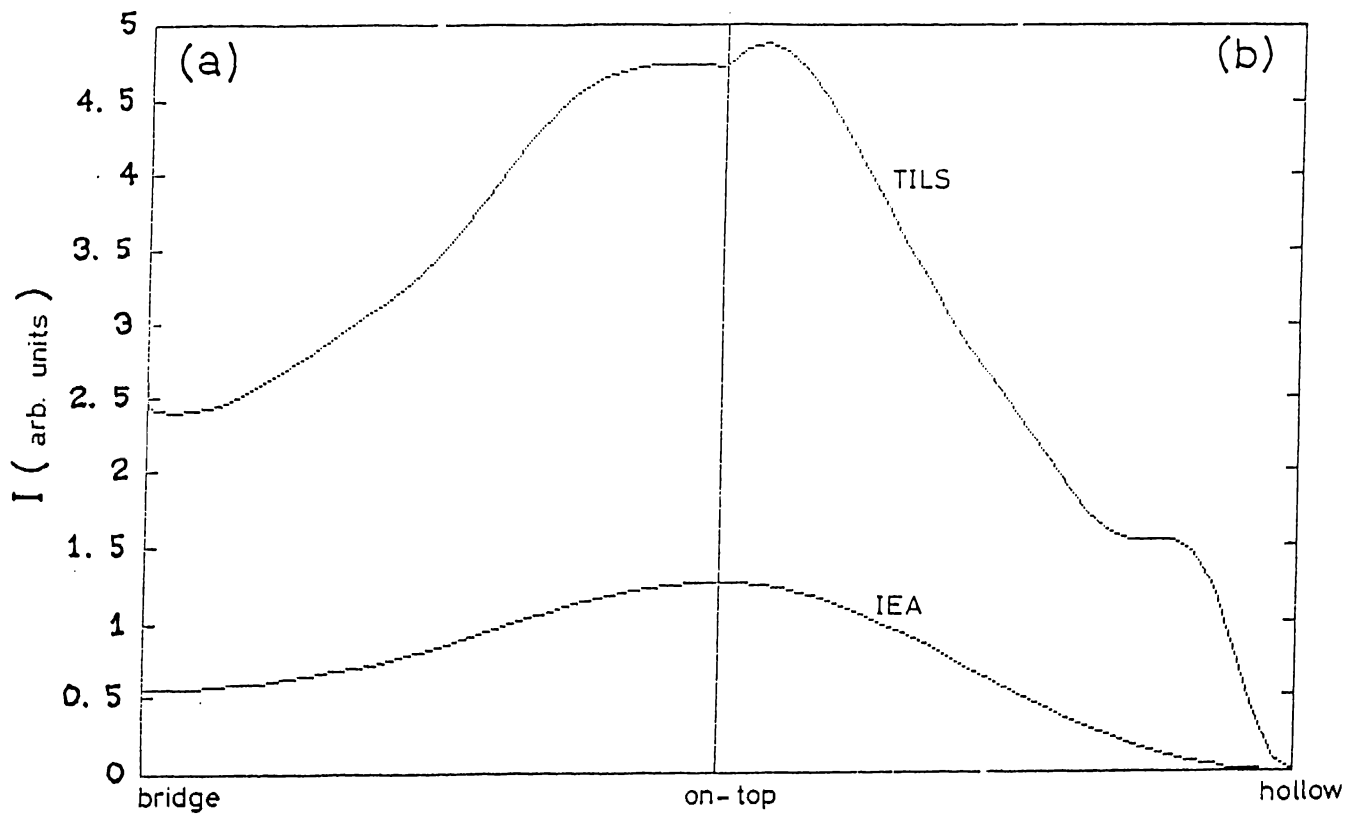

Figure 4.6: Tunneling current along special directions

The tip height is taken to be equal to 2.0 Å.

The results show that there is a strong enhancement in the tunneling current as a result of the tip-surface interaction. This point explains the effects of this intercation on the large corrugation observed for graphite. When the tip is above some point other than the hollow-site it can not come closer to the surface than a special cut-off distance beyond which current is enhanced due to the presence of the Tip Induced Localized States. However around the hollow-site practically there is no tip-surface interaction that would lead to a jump in the current, which would block the tip. There the tip can come close to surface to attain the prescribed constant current. This mechanism can lead to corrugations up to $\sim 3 - 4$ Å depending on the bias. When the bias is large, first there is no need to be close to the surface to obtain the constant current, and second the Tip Induced States will not be this effective due to the lifted degeneracy.

Chapter 5

Conclusions and Discussion

In this study I investigated the atomic nature of Scanning Tunneling Microscopy. Some experiments are carried out so far for extremely small tip heights for some special structures. Such small separation operation is rather different from that of the large separation regime. In the latter by using detailed microscopic knowledge about the electrodes, one can find the tunneling current easily as a result of the independent tip and surface. This case was analyzed by several researchers.

For the small separation case, the tip and the surface atoms have internuclear separations of the order of nearest-neighbor distance for the original electrodes. For this case there appears a possibility of the existence of some localized states at the vicinity of the tip. This basic idea is a direct consequence of the chemisorption theory. In order to determine and identify these localized states, it is necessary to have the information about the microscopical structure of the tip. Even in the state-of-the-art studies this is not fully possible. Therefore, it is necessary to make some simplifying, still

realistic approximations.

For the simplicity of its structure and for its wide applications in Scanning Tunneling Microscopy, I have chosen the graphite (0001) surface as the sample substrate. As a result of its very anisotropic structure only a monolayer is taken to represent the graphite surface. The tip in turn is defined by a single atom, which is thought to be in a jelium-like background in order to complete the electrical connections. The interaction parameters are again not determined from the first principles, due to the lack of information about the real tip. The electronic energy bands are calculated by using the Empirical Tight Binding method.

Calculating the electronic band structure for several structures it is found that the combined system can belong to one of three regimes:

- Chemical binding regime in which the tip and the surface are in physical contact. The band structure does not resemble original ones as a result of strong interaction.

- Tip Induced Localized States regime in which there is a non-zero interaction between the tip and the surface, but not strong enough to connect the two electrodes chemically. The so-called Tip Induced Localized States are hybrid combinations of the original tip orbitals and the surface states.

90

- Independent electrode regime in which the interaction between the tip and the surface is negligibly small. The previous studies on Scanning Tunneling Microscopy used the underlying results which are particular to this regime.

It is found that the presence and the character of the Tip Induced Localized States depend of the lateral position of the tip, in addition to its height. While at the on-top site the Tip Induced Localized States are most effective, there are no such states at the hollow-site position.

The Golden-rule expression of Bardeen for tunneling is modified to include the effects of the Tip Induced Localized States on tunneling. It is found that there is an enhancement of the current as a result of the states of the combined system. For graphite it is shown that the current increases by a factor > 4 in the Tip Induced Localized States regime.

This final result can partly explain the observed giant corrugations for graphite. Due to the presence of the Tip Induced Localized States the tunneling current becomes equal to the local density prediction up to a few Å's above the expected position from the local density calculations. Thus even though the corrugation of the local density of states is small, the observed corrugation may be large.

Owing to the limited information about the tip structure, the calculations

cannot be carried out from the first principles. The parameters and functions are used by some simple scaling and fitting procedures.

The concept of Tip Induced Localized States which is proposed for graphite, can be used for all structures, for which the tip comes close to the sample surface. The natural candidates are semiconductors and the charge-density wave structures.

As the final conclusion of this study one can say that the tip-surface interaction in Scanning Tunneling Microscopy is one of the basic aspects, which has to be taken into account for a correct description of the problem.

References

[1] J.R. Oppenheimer. *Three Notes on the Quantum Theory of Aperiodic Effects.* **Physical Review**, 31:66, 1928.

[2] R.H. Fowler and L. Nordheim. *Electron Emission in Intense Electric Fields.* **Procceedings of Royal Society, London, Serie A**, 119:173, 1928.

[3] C.B. Duke. *Tunneling in Solids, Solid State Physics. Supplement 10.* Academic Press, 1969.

[4] J. Frenkel. *On the Electrical Resistance of Contacts Between Solid Conductors.* **Physical Review**, 36:1604, 1930.

[5] L. Esaki. *New Phenomenon in Narrow Germanium p-n Junctions.* **Physical Review**, 109:603, 1958.

[6] G. Binnig, H. Rohrer, Ch. Gerber, and E. Weibel. *Surface Studies by Scanning Tunneling Microscopy.* **Physical Review Letters**, 49:57, 1982.

[7] G. Binnig and H. Rohrer. *Scanning Tunneling Microscopy.* **Helvetica Physica Acta**, 55:726, 1982.

[8] G. Binnig, H. Rohrer, Ch. Gerber, and E. Weibel. *Tunneling Through a Controllable Vacuum Gap.* **Applied Physics Letters**, 40:178, 1982.

[9] G. Binnig, H. Rohrer, Ch. Gerber, and E. Weibel. *Vacuum Tunneling.* **Physica**, 109:2075, 1982.

[10] G. Binnig and H. Rohrer. *Scanning Tunneling Microscopy.* **IBM Journal of Research and Development**, 30:355, 1986.

[11] J. Bardeen. *Tunneling From a Many-Particle Point of View.* **Physical Review**, 6:57, 1961.

[12] O.J. Marti. *Scanning Tunneling Microscopy at Low Temperatures.* PhD thesis, Swiss Federal Institute of Technology, Zurich, 1986.

[13] A.M. Baro, R. Miranda, J. Alaman, N. García, G. Binnig, H. Rohrer, Ch. Gerber, and J.L. Carrascosa. *Determination of Surface Topography of Biological Specimens at High Resolution by Scanning Tunneling Microscopy.* **Nature**, 315:253, 1983.

[14] Sang-Il Park and C.F. Quate. *Tunneling Microscopy of Graphite in Air.* **Applied Physics Letters**, 48:112, 1986.

[15] R. Sonnenfeld and P.K. Hansma. *Atomic Resolution Microscopy in Water.* **Science**, 232:211, 1986.

[16] B. Drake, R. Sonnenfeld, J. Schneir, and P.K. Hansma. *Scanning Tunneling Microscopy of Processes at Liquid-Solid Interfaces.* **Surface Science**, 181:92, 1987.

[17] J. Schneir, R. Sonnenfeld, P.K. Hansma, and J Tersoff. *Tunneling Microscopy Study of the Graphite Surface in Air and Water.* **Physical Review,** B 34:4979, 1986.

[18] G. Binnig, H. Rohrer, Ch. Gerber, and E Weibel. *(111) Facets as the Origin of Reconstructed Au(110).* **Surface Science,** 131:L379, 1983.

[19] G.K. Binnig, H. Rohrer, Ch. Gerber, and E Stoll. *Real-space Observation of the Reconstruction of Au(100).* **Surface Science,** 144:321, 1984.

[20] G. Binnig, H. Rohrer, Ch. Gerber, and E. Weibel. 7×7 *Reconstruction on Si(111) Resolved in Real Space.* **Physical Review Letters,** 50:120, 1983.

[21] L.C. Snyder, Z. Wassermann, and J.W. Moskowitz. *Milk-Stoll Model for Si(111) Surface Reconstruction.* **Journal of Vacuum Science and Technology,** 16:1266, 1979.

[22] W.A. Harrison. *Surface Reconstruction on Semiconductors.* **Surface Science,** 55:1, 1976.

[23] J.M. Soler, A.M. Baro, N. García, and H. Rohrer. *Interatomic Forces in Scanning Tunneling Microscopy: Giant Corrugations of the Graphite Surface.* **Physical Review Letters,** 57:444, 1986.

[24] A. Bryant, D.P.E. Smith, G. Binnig, W.A. Harrison, and C.F. Quate. *Anomalous Distance Dependence in Scanning Tunneling Microscopy.* **Applied Physics Letters,** 49:936, 1986.

[25] D. Tománek, S.G. Louie, J. Mamin, D.W. Abraham, R.E. Thomson, E. Ganz, and J Clarke. *Theory and Observation of Highly Asymmetric Atomic Structure in Scanning Tunneling Microscopy Images of Graphite.* **Physical Review**, B 35, 19876.

[26] I.P. Batra, N. García, H. Rohrer, H. Salemink, E. Stoll, and S. Ciraci. *A Study of Graphite Surface with STM and Electronic Structure Calculations.* **Surface Science**, 181:126, 1987.

[27] G. Binnig. *Scanning Tunneling Microscopy.* 1987. Invited Talk, 7th General Conference of the Condensed Matter Division, EPS; to be published in Physica Scripta.

[28] Y. Kuk and P.J. Silverman. *Role of Tip Structure in Scanning Tunneling Microscopy.* **Applied Physics Letters**, 48:1597, 1986.

[29] R.V. Coleman, B. Drake, P.K. Hansma, and G. Slough. *Charge-Density Waves Observed with a Tunneling Microscopy.* **Physical Review Letters**, 55:394, 1985.

[30] N. García, C. Ocal, and F. Flores. *Model Theory for Scanning Tunneling Microscopy: Application to Au(110)(1×2).* **Physical Review Letters**, 50:2002, 1983.

[31] E. Stoll, A. Baratoff, A. Selloni, and P. Carnevali. *Current Distribution in the Scanning Vacuum Tunnel Microscope: A Free-electron Model.* **Journal of Physics**, C 17:3073, 1984.

[32] J. Tersoff and D.R. Hamann. *Theory of the Scanning Tunneling Microscope.* **Physical Review**, B 31:805, 1985.

[33] J. Tersoff and D.R. Hamann. *Theory of the Scanning Tunneling Microscope.* **Physical Review**, B 31:805, 1985.

[34] M.S. Chung, T.E. Feuchtwang, and P.H. Cutler. *Spherical Tip Model in the Theory of the Scanning Tunneling Microscope.* **Surface Science**, 187:559, 1987.

[35] C.J. Chen. *Theory of Scanning Tunneling Spectroscopy I.* 1987. unpublished.

[36] T.E. Feuchtwang, P.H. Cutler, and N.M. Miskovsky. *A Theory of Vacuum Tunneling Microscopy.* **Physics Letters**, A 99:167, 1983.

[37] A. Baratoff. *Theory of Scanning Tunneling Microscopy-Methods and Approximations.* **Physica**, B 127:143, 1984.

[38] T.E. Feuchtwang and P.H. Cutler. *Tunneling and Scanning Tunnel Microscopy: A Critical Review.* **Physica Scripta**, 35:132, 1987.

[39] N.D. Lang. *Electronic Structure and Tunneling Current for Chemisorbed Atoms.* **IBM Journal of Research and Development**, 30:374, 1986.

[40] N.D. Lang. *Theory of Single-atom Imaging in the Scanning Tunneling Microscopy.* **Physical Review Letters**, 56:1164, 1986.

[41] N.D. Lang. *Vacuum Tunneling Current from an Adsorbed Atom.* **Physical Review Letters**, 55, 1985.

[42] G. Doyen and D. Drakova. *Model Calculations for the Tunneling Current froma Tungsten Tip to a Flat and Stepped Nickel(100) Surface.* **Surface Science**, 178:375, 1986.

[43] R.C. Tatar and S. Rabii. *Electronic Properties of Graphite: A Unified Approach.* **Physical Review**, B 25:4126, 1982.

[44] M. Tinkham. *Group Theory and Quantum Mechanics*, chapter 4. Mc Graw Hill, New York, 1964.

[45] G.S. Painter and D.E. Ellis. *Electronic Band Structure and Optical Properties of Graphite from a Variational Approach.* **Physical Review**, B 1:4747, 1970.

[46] M Yamazaki. *Electronic Band Structure in Graphite.* **Journal of Chemical Physics**, 26:930, 1957.

[47] H.-W. Fink. *Mono-atomic Tips for Scanning Tunneling Microscopy.* **IBM Journal of Research and Development**, 30:460, 1986.

[48] A. Selloni, P. Carnevali, E. Tosatti, and C.D. Chen. *Voltage-dependent Scanning-tunneling Microscopy of a Crystal Surface: Graphite.* **Physical Review**, B 31:2602, 1985.

[49] I.P. Batra and S. Ciraci. *Theoretical Scanning Tunneling Microscope and Atomic Force Microscope Study of Graphite Including Tip-Surface Interaction.* 1987. Presented in STM'87; to be published in Journal of Vacuum Science and Technology.

[50] J. Tersoff. *Anomalous Corrugations in Scanning Tunneling Microscopy: Imaging of Individual States.* **Physical Review Letters**, 57:440, 1986.

[51] S. Ciraci and I.P. Batra. *Scanning Tunneling Microscopy at Small Tip to Surface Distances.* **Physical Review**, B 36:6194, 1987.

[52] H.A. Mizes, Sang-Il Park, and W.A. Harrison. *A Multiple Tip Interpretation of Anomalous Scanning Tunneling Microscopy Images of Layered Materials.* **Physical Review**, B 36:4497, 1987.

[53] W.A. Harrison. *Electronic Structure and the Properties of Solids,* chapter 6. W. H. Freeman and Company, San Fransisco, 1980.

[54] J.C. Slater and G.F. Koster. *Simplified Linear Combination of Atomic Orbitals Method for the Perioidic Potential Problem.* **Physical Review**, 94:1498, 1954.

[55] E. Clementi and D.L. Raimondi. *Atomic Screening Constants from SCF Functions.* **Journal of Chemical Physics**, 48:2686, 1963.

[56] E. Tekman and S. Ciraci. *Tip Induced Localized States in Scanning Tunneling Microscopy.* 1987. to be published in Physica Scripta.